methods and protocols

MDPI

Article

Comparison of Dual-Luciferase® Reporter Assay and a Stably Transfected NF-κB Reporter Cell Line for Detecting TNF-α and X-Ray-Induced Pathway Activation

Sebastian Feles [1,2,*,†], Sebastian Diegeler [2,†,‡], Bernd Henschenmacher [2,3], Christa Baumstark-Khan [2] and Christine Elisabeth Hellweg [2]

[1] Aeromedical FabLab, Institute of Aerospace Medicine, German Aerospace Center (DLR), 51147 Cologne, Germany
[2] Radiation Biology, Institute of Aerospace Medicine, German Aerospace Center (DLR), 51147 Cologne, Germany; sd2085@cam.ac.uk (S.D.); bhenschenmacher@bfs.de (B.H.); christa.baumstark-khan@dlr.de (C.B.-K.); christine.hellweg@dlr.de (C.E.H.)
[3] Bundesamt für Strahlenschutz (BfS)—Federal Office for Radiation Protection, Optical Radiation, 85764 Oberschleißheim, Germany
* Correspondence: sebastian.feles@dlr.de
† These authors contributed equally to this work.
‡ Current address: Department of Pathology, University of Cambridge, Cambridge CB2 1QP, UK.

Abstract

The transcription factor nuclear factor kappa B (NF-κB) is a central regulator of inflammatory and genotoxic stress responses and is involved in immune function and disease pathogenesis. Reporter assays are widely used to quantify NF-κB activation, yet systematic benchmarks between transient dual-luciferase and stable fluorescent formats under harmonized conditions are lacking. We compared a transient Dual-Luciferase® Reporter (DLR™) assay in HEK293 cells with the stably transfected HEK-pNF-κB-d2EGFP/Neo L2 cell line using recombinant TNF-α and X-rays as stimuli. Dynamic range, limit of detection (LOD), signal-to-noise ratio (S/N), and half-maximal effective concentrations and doses (EC_{50}, ED_{50}) were derived from four-parameter logistic modeling. The HEK-pNF-κB-d2EGFP/Neo L2 line showed higher sensitivity to TNF-α (EC_{50} = 0.31 ng/mL) than the DLR™ assay (1.2–2.0 ng/mL) and a lower LOD, whereas the DLR™ assay provided better temporal resolution, revealing assay-specific signal decline attributable to reporter stability and readout kinetics. For X-ray exposure, both systems showed comparable potency (EC_{50} ≈ 5–8 Gy), while the stable cell line maintained superior S/N. Both reporter systems support high-throughput and mechanistic applications: the DLR™ assay offers versatility across cell types, while the HEK-pNF-κB-d2EGFP/Neo L2 line provides higher sensitivity, dynamic range, and single-cell resolution.

Keywords: NF-κB reporter assay; Dual-Luciferase Reporter® assay; destabilized enhanced green fluorescent protein; transient transfection; stable transfection; assay sensitivity; dynamic range; human embryonic kidney cells

Academic Editor: Philip Hublitz

Received: 26 November 2025
Revised: 20 January 2026
Accepted: 22 October 2026
Published: 9 November 2026

Copyright: © 2026 by the authors. Licensee MDPI, Basel, Switzerland. This article is an open access article distributed under the terms and conditions of the Creative Commons Attribution (CC BY) license.

1. Introduction

The transcription factor NF-κB (nuclear factor kappa-light-chain-enhancer of activated B cells) is a key regulator of innate and adaptive immune responses, inflammation,

cell growth and survival [1–3]. NF-κB can be activated by inflammatory stimuli, oxidative stress, and genotoxic insults, including ionizing radiation [4–6]. As a hallmark of proinflammatory signaling, NF-κB activation has been extensively studied in contexts ranging from inflammation [3,7], infections [8,9], immune regulation [1] and apoptosis resistance to cellular transformation, cancer progression and therapy resistance [10,11]. Consequently, quantitative and dynamic measurement of NF-κB activation is a central methodological requirement in cancer research, immunology, molecular toxicology, radiobiology, and high-throughput screening [12–14].

Reporter assays provide a useful approach to monitor cellular processes with straightforward and quantifiable readouts. Importantly, their performance and interpretability are inherently context-dependent and influenced by the cellular system in which they are applied. They rely on transient or stable transfection of plasmids or viral delivery systems (e.g., lenti- or retroviral vectors) carrying the reporter gene under the control of the promoter or enhancer element of interest [15]. Reporter genes encode fluorescent proteins or enzymes such as luciferase. To control for the transfection efficiency in transient transfection-based reporter assays, a second plasmid encoding a different reporter gene under the control of a constitutively active promoter can be transfected; the expression of the second reporter is monitored and used for normalization. This approach was realized by the Dual-Luciferase Reporter Assay (DLR™ assay; Promega, Madison, WI, USA). It enables sensitive and rapid detection of NF-κB activation by co-expressing firefly luciferase under NF-κB control and a constitutively expressed *Renilla* luciferase for ratiometric normalization on viable and successfully transfected cells [16,17]. This configuration overcomes limitations of single-reporter assays, such as the need for split samples or parallel transfections, and is reported to provide high precision, minimal signal interference, and linearity over seven to eight orders of magnitude [18].

As an alternative, NF-κB–responsive constructs were integrated into the host genome of stably transfected reporter lines, eliminating variability of transient transfection and enabling prolonged or repeated stimulations [19,20]. The HEK-pNF-κB-d2EGFP/Neo L2 line, developed as described in Hellweg et al. [21], expresses destabilized enhanced green fluorescent protein (d2EGFP) under NF-κB control. Incubation of this cell line with well-known NF-κB activators such as tumor necrosis factor α (TNF-α), interleukin -1β and phorbol 12-myristate 13-acetate (PMA) resulted in concentration-dependent upregulation of NF-κB-controlled d2EGFP expression [22]. Exposure to DNA double-strand breaking agents such as camptothecin, X-rays and energetic heavy ions also resulted in dose-dependent reporter gene expression [22,23]. Such HEK293-based reporter systems provide a robust and experimentally tractable model to study NF-κB activation under defined conditions, while not aiming to recapitulate cell-type-specific signaling responses observed in primary or specialized cells [24].

Despite their widespread use, these two reporter assay formats have not been systematically compared under harmonized, assay-specific experimental endpoints. Critical performance characteristics—dynamic range, sensitivity, assay variability, throughput, and suitability for screening—remain undocumented in a direct head-to-head assessment. Addressing this gap is particularly relevant for new approach methodologies (NAMs) for in vitro toxicology and radiation biology, where assay robustness, scalability, and operational efficiency are decisive selection criteria.

Here, we present a direct, pragmatic comparison at defined experimental readout endpoints of transiently transfected DLR™ reporter plasmids in HEK293 cells and the HEK-pNF-κB-d2EGFP/Neo L2 cell line for quantifying NF-κB activation in response to TNF-α and X-ray exposure. By standardizing culture conditions, stimulation protocols, and readout parameters, we assess strengths and limitations of each system and provide guidance for assay selection based on sensitivity, precision, and practical deployment in

screening and mechanistic studies. This study addresses the lack of a standardized, quantitative benchmark between transient dual-reporter assays and stable NF-κB reporter cell lines, aiming to define their respective performance envelopes and operational trade-offs to support evidence-based assay selection in both high-throughput and mechanistic research contexts.

Accordingly, this study focuses on the comparison of two widely used NF-κB reporter implementations within a defined HEK293-based model system, rather than on a universal methodological evaluation of luminescence- versus fluorescence-based reporter technologies.

2. Material and Methods

2.1. Materials

A comprehensive list of all reagents, cell lines, plasmids, and equipment used in this study is provided in Table 1. This overview follows the Key Resources Table format to facilitate reproducibility. Recipes for cell culture media and buffers are listed in Table 2.

Table 1. Key Resources.

Reagent or Resource	Source	Identifier
Chemicals, peptides, and recombinant proteins		
Human tumor necrosis factor-alpha (TNF-α), recombinant	Sigma-Aldrich, Steinheim, Germany	Cat No H8916-10UG
G418 (Geniticin)	Sigma-Aldrich, Steinheim, Germany	Cat No G8168-10ML, CAS 108321-42-2
Formaldehyde 37% in H_2O	Sigma-Aldrich, Steinheim, Germany	Cat No 252549, CAS 50-00-0
NaCl	Sigma-Aldrich, Steinheim, Germany	Cat No S9888
KCl	Sigma-Aldrich, Steinheim, Germany	Cat No P3911
$Na_2HPO_4 \times 7\ H_2O$	Sigma-Aldrich, Steinheim, Germany	Cat No S9390
KH_2PO_4	Sigma-Aldrich, Steinheim, Germany	Cat No P0662
Commercial assays		
Firefly luciferase vector pGL4.32 [luc2P/NF-κB-RE/Hygro]	Promega, Madison, WI, USA	Cat No E8491
Renilla luciferase vector pGL4.75 [hRluc/CMV] (CMV promoter-driven)	Promega, Madison, WI, USA	Cat No E6931
FuGENE® HD Transfection Reagent	Promega, Madison, WI, USA	Cat No E2311
Dual-Luciferase Reporter DLR™ Assay System	Promega, Madison, WI, USA	Cat No E1910
Experimental models: Cell lines		
HEK293 (immortalized human embryonal kidney)	LGC Standards, Wesel, Germany	ATCC CRL-1573

HEK-pNF-κB-d2EGFP/Neo L2	Generated previously as described in Hellweg et al. (2003)	[21]
Software and algorithms		
i-control™	Tecan, Männedorf, Switzerland	version 3.4.2.0
CellQuest Pro	BD Biosciences, San Jose, CA, USA.	version 1.2
GraphPad Prism	GraphPad Software, San Diego, CA, USA	version 10.5.0
RStudio	[25]	version 2025. 5.1.513
R	[26]	version 4.4.3
R Packages		
clipr	[27]	version 0.8.0
colorspace	[28]	version 2.1-1
dplyr	[29]	version 1.1.4
drc	[30]	version 3.0.1
forcats	[31]	version 1.0.0
ggplot2	[32]	version 3.5.2
glue	[33]	version 1.8.0
lubridate	[34]	version 1.9.4
patchwork	[35]	version 1.3.2
purrr	[36]	version 1.1.0
readr	[37]	version 2.1.5
readxl	[38]	version 1.4.5
renv	[39]	version 1.1.4
scales	[40]	version 1.4.0
stringr	[41]	version 1.5.1
tibble	[42]	version 3.3.0
tidyr	[43]	version 1.3.1
tidyverse	[44]	version 2.0.0
writexl	[45]	version 1.5.4
Instruments		
RS225 X-ray Generator		Gulmay Medical (now X-Strahl), Surrey, UK
UNIDOS^{webline} dosimeter and ionization chamber Type TM30013		PTW, Freiburg, Germany
Infinite 200 Pro, Multimode plate Reader, Dual-injectors, reference 30050303		Tecan, Crailsheim, Germany
Components for Infinite 200 Pro V_2.10_00/2007 incl. heating elements, injectors and emission filter wheel for luminescence measurement		Tecan, Crailsheim, Germany
FACScan Flow Cytometer		BD Biosciences, San Jose, CA, USA
Media and Buffers		
α-MEM Eagle media	Pan Biotech, Aidenbach, Germany	Cat No P04-21050

Penicillin (10.000 U/mL) -Streptomycin (10 mg/mL)	Pan Biotech, Aidenbach, Germany	Cat No P06-07100
Fetal Bovine Serum (FBS)	Pan Biotech, Aidenbach, Germany	Cat No P40-37500
Trypsin 0.05%/EDTA 0.02% in DPBS, w/o: Ca and Mg	Pan Biotech, Aidenbach, Germany	Cat No P10-023100
Consumables		
Culture flasks, 25 cm^2	LABSOLUTE, Th.Geyer, Renningen, Germany	Cat No 7696781
Culture flasks, 75 cm^2	LABSOLUTE, Th.Geyer, Renningen, Germany	Cat No 7696782
35 mm Nunc, Delta-Treated Cell culture dishes	Thermo Fisher Scientific, Waltham, MA, USA	Cat No 150460
Nunc™ MicroWell™ 96-Well, Nunclon Delta-Treated, Flat-Bottom Microplate	Thermo Fisher Scientific, Waltham, MA, USA	Cat No 167008
Pierce™ 8-Well Polystyrene Strip Plates, Corner Notch	Thermo Fisher Scientific, Waltham, MA, USA	Cat No 15031

Table 2. Buffer and media recipes.

Buffer/Media	Ingredients
α-MEM without supplements	α-MEM Eagle media
α-MEM complete media	10% (*v*/*v*) FBS 100 U/mL Penicillin, 100 µg/mL Streptomycin in α-MEM Eagle media
α-MEM selection media	1.5 mg/mL G418 in α-MEM complete media
Phosphate buffered saline (PBS)	137 mmol/L NaCl 2.3 mmol/L KCl 4.3 mmol/L $Na_2HPO_4 \times 7\ H_2O$ 1.4 mmol/L KH_2PO_4 in ddH_2O

2.2. Cell Culture

The human embryonic kidney cell line HEK293 was originally established by Graham et al. [46] via transfection with adenovirus type 5 DNA fragments and contains the integrated E1A and E1B regions without producing viral particles. Cells were routinely cultured in α-MEM complete medium in 75 cm^2 cell culture flasks.

The cell line HEK-pNF-κB-d2EGFP/Neo L2 is a HEK293 derivative that was generated via stable transfection with the plasmid pNF-κB-d2EGFP/Neo. This construct contains four tandem repeats of the NF-κB response element upstream of a minimal promoter controlling expression of a destabilized enhanced green fluorescent protein (d2EGFP) and a neomycin phosphotransferase II (neo) resistance gene conferring geneticin (G418) resistance for clonal selection under the control of the constitutive SV40 enhancer [21]. The genomic integration copy number of the NF-κB–d2EGFP reporter cassette in clone L2 has not been explicitly reported in the original cell line description. The cell line was maintained in α-MEM selection media in 75 cm^2 cell culture flasks and passaged once per week.

All cultures were maintained under standard incubator conditions at 37 °C in a humidified atmosphere of 95% air and 5% CO_2.

2.3. Transient Transfection and Dual-Luciferase Reporter (DLR™) Assay

The NF-κB reporter plasmid used for the DLR™ assay, pGL4.32[luc2P/NF-κB-RE/Hygro], encodes a destabilized firefly luciferase (luc2P) under the control of a synthetic promoter containing five tandem repeats of the NF-κB response element positioned upstream of a minimal TATA box. This promoter configuration enables strong, inducible transcriptional activation in response to NF-κB signaling while maintaining low basal activity [47].

For transient transfection of the DLR™ assay reporter plasmids, HEK293 cells were seeded at a density of 1.1×10^4 cells per well ($3.7 \times 10^4/cm^2$) in flat-bottom 96-well plates and incubated at 37 °C for 72 h until ~75% confluency was reached (Figure 1A). Prior to transfection, culture media was replaced with 100 µL α-MEM without supplements. Cells were co-transfected with the firefly luciferase NF-κB reporter plasmid and control *Renilla* luciferase vector using FuGENE HD Transfection Reagent, following manufacturer instructions. The ratio of the two vectors was 4.8:1 (NF-κB:*Renilla*) based on DNA weight.

For one 96-well plate, 483 µL α-MEM were combined with 8.7 µg of NF-κB reporter plasmid DNA (pGL4.32 [luc2P/NF-κB-RE/Hygro]; 1 µg/µL stock, 8.7 µL), 1.8 µg of CMV-*Renilla* control plasmid DNA (pGL4.75 [hRluc/CMV]; 1 µg/µL stock, 1.8 µL), and 31.5 µL FuGENE HD transfection reagent. The mixture was gently pipetted to ensure homogeneity and incubated for 10 min at room temperature to allow complex formation. Subsequently, 5 µL of the transfection mix was dispensed into each well containing 100 µL of preloaded media. After transfection, cells were incubated at 37 °C for 24 h and exposed to TNF-α or X-rays as described in Sections 2.5 and 2.6, respectively.

NF-κB activation was assessed using the DLR™ assay according to the manufacturer's manual [18]. Before measurement, culture media was removed and wells were gently washed with PBS to remove residuals. Then 20 µL of 1× Passive Lysis Buffer was added per well and incubated for 15 min at room temperature to ensure uniform coverage and complete lysis, before lysates were collected for measurement. The 5× Passive Lysis Buffer stock was diluted to 1× immediately before use.

Luminescence was quantified using a Tecan Infinite 200 Pro multimode plate reader equipped with dual injectors and set to a target temperature of 30 °C. The injection and measurement script consisted of sequential injection of 100 µL Luciferase Assay Reagent II (LAR II) to generate firefly luciferase signal and 100 µL Stop & Glo® Reagent to quench firefly luciferase and induce *Renilla* luciferase signal, with a 2-s delay before signal acquisition. Firefly and *Renilla* luciferase signals were recorded for 1000 ms each in duplicate channels (Label1/Label3 and Label2/Label4, respectively) due to the instrument's scripting protocol, which assigns two parallel labels per reporter for technical redundancy. Both channels correspond to the same optical filter set. The integrated filters BLUE1 (440/40 nm; Label3/Label4) and GREEN (545/25 nm; Label1/Label2) were used. Firefly luminescence was divided by *Renilla* luminescence in each well to normalize the NF-κB-dependent luminescence signal to the number of viable, successfully transfected cells, resulting in the relative NF-κB response. This dual-reporter normalization approach compensates for well-to-well variability in transient transfection efficiency and cell number, as recommended by the assay manufacturer. Detection time points were selected based on established reporter-specific response characteristics [18,47].

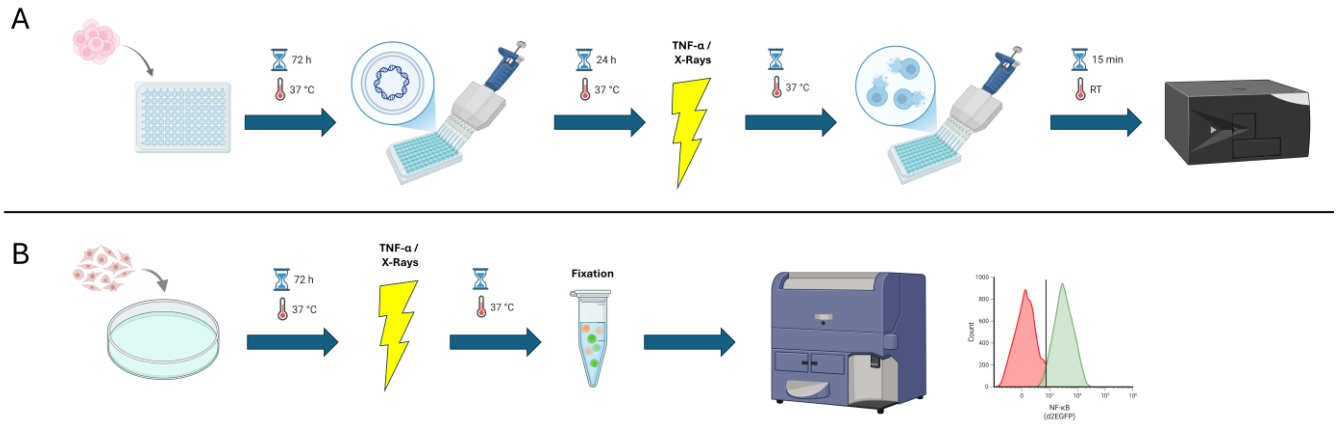


Figure 1. Workflow of the two NF-κB reporter assay formats compared in this study. The schematic illustrates the experimental sequence for (**A**) the transiently transfected Dual-Luciferase® Reporter (DLR™) assay in HEK293 cells and (**B**) the stably transfected HEK-pNF-κB-d2EGFP/Neo L2 reporter cell line. The flow chart outlines cell seeding, transfection or maintenance, stimulation with TNF-α or X-rays, and subsequent signal detection by luminescence reading or flow cytometry of green fluorescence. All steps were conducted under harmonized culture and stimulation conditions to ensure direct comparability of assay performance.

2.4. Preparation of the Stably Transfected Cell Line

For stimulation, HEK-pNF-κB-d2EGFP/Neo L2 cells were seeded into cell culture dishes (∅ 35 mm) at a density of 2 × 10^4 cells/cm^2 and cultured for 72 h (Figure 1B) in α-MEM complete before exposure to TNF-α or X-rays, as described in Sections 2.5 and 2.6, respectively.

2.5. Stimulation with TNF-α

TNF-α was reconstituted in PBS (1 µg/mL) and final dilutions were prepared in α-MEM complete. Final concentrations for the DLR™ assay were 0, 0.625, 1.25, 2.5, 5 and 10 ng/mL, with 16 technical replicates per condition. Stimulation was performed at 37 °C for 3, 5, 8.5, 15 or 24 h followed by immediate lysis and luciferase measurement as described in Section 2.3.

Final concentrations for treatment of the HEK-pNF-κB-d2EGFP/Neo L2 cells were 0, 0.05, 0.0625, 0.1, 0.125, 0.25, 0.5, 1, 5 and 10 ng/mL with 3 technical replicates per condition. Cells were stimulated for 20 h and then processed for flow cytometry as described in Section 2.6.

2.6. Irradiation with X-Rays

Cells in their respective vessel were exposed to 0, 1, 2, 4, 8, 16 and 32 Gy X-rays at room temperature using an RS225 X-ray generator at 200 kV and 15 mA, equipped with a 0.5 mm copper filter to remove low-energy X-rays, resulting in a dose-averaged linear energy transfer (LET) of 0.3–3.0 keV/µm. A fixed source-to-sample distance of 420 mm yielded a constant dose rate of 1.0 Gy/min.

Dosimetry was performed during each experiment with an ionization chamber of the type TM30013 connected to the dosimeter UNIDOS^{webline}. Dose ranges were assay-specific and are reported accordingly.

For the DLR™ assay, irradiation with doses of 0–32 Gy was performed in 96-well strip-well plates (8-well removable format), enabling separate exposure of selected strips. Doses were applied to transfected cells in strips that were removed from the 96-well-plate frame, with 16 technical replicates per condition. Following exposure, irradiated media was exchanged with fresh α-MEM complete, and cells were incubated at 37 °C for 5 or 8.5

h before the DLR™ assay. An exploratory measurement at 32 Gy (5 h post-irradiation, n = 1) was not used for comparison between assays.

For the HEK-pNF-κB-d2EGFP/Neo L2 cell line, doses of 0–16 Gy were applied to cells in cell culture dishes (∅ 35 mm), medium was exchanged, and cells were incubated at 37 °C for 18 h before preparation for flow cytometry.

2.7. Quantification of d2EGFP Fluorescence by Flow Cytometry

For flow cytometric assessment of d2EGFP expression, cells were detached using Trypsin/EDTA and immediately fixed in 3.5% formaldehyde in PBS. Cells were then washed and resuspended with PBS. Using a BD FACScan Flow Cytometer with a 488 nm laser, events were gated as "cells" in Cell Quest Pro using forward and side scatter (FSC, SSC). In this gate, d2EGFP fluorescence was measured in the FL1 channel (emission band-pass filter 530/30 nm). Events were defined as negative for NF-κB-dependent d2EGFP expression in the untreated control, setting a threshold containing the lowest > 95% of the events in the population. This threshold was applied to all samples for assessment of events positive for NF-κB-dependent d2EGFP expression. The percentage of d2EGFP-positive cells was used as a readout for NF-κB activation. For comparison with the DLR™ assay, the percentage of d2EGFP-positive cells of the treated samples was normalized to the respective percentage in the untreated cells (baseline), resulting in the relative NF-κB response. Each experiment used 3 technical replicates per condition and was repeated independently 2–10 times. Detection time points were selected based on established reporter-specific response characteristics [21].

2.8. Data Analysis

All quantitative analyses were performed using R version 4.4.3 and RStudio version 2025.5.1.513. For each assay type, reporter signal data (firefly/*Renilla* luminescence ratios for the DLR™ assay or percentages of d2EGFP-positive cells for the HEK-pNF-κB-d2EGFP/Neo L2 line) were averaged across technical replicates to obtain mean response values for each concentration or dose. The baseline was defined as the mean response of all untreated control samples (0 ng/mL TNF-α or 0 Gy X-rays, respectively). The maximal response (Max Response) was defined as the highest measured mean response value within the tested concentration or dose range. Fold induction was calculated as the ratio of the mean response value at a given concentration or dose to the baseline value. Dynamic range was defined as fold change at Max Response.

Dose-response modelling was performed using the R package "drc" by nonlinear regression using a four-parameter logistic (4PL) model:

$$Y = Bottom + \frac{Top - Bottom}{1 + (\frac{EC_{50}}{X})^{HillSlope}} \quad (1)$$

where Bottom and Top represent lower and upper asymptotes, EC_{50} denotes the concentration or dose producing 50% of the maximal modelled response, and Hill slope describes the curve's steepness [48]. Independent fits were performed for each assay dataset, defining Max Response as Top and baseline as Bottom. For graphical presentation, the X-axis was transformed to a symlog scale, linear from 0 to 0.1 and $\log_{10}$-transformed for larger values to improve visualization of the response range. Models were fitted using ordinary least squares without weighting, with EC_{50} constrained to values > 0. Ninety-five percent confidence intervals (95% CI) for all parameters were derived from asymptotic standard errors (SE) obtained from the covariance matrix of the fit.

EC_{50} value and Hillslope were extracted from the same regression analysis. Signal-to-noise ratio (S/N) was calculated for EC_{50}:

$$S/N_{EC_{50}} = \frac{Signal_{EC_{50}} - Signal_{baseline}}{SD_{baseline}} \quad (2)$$

with a S/N > 3 considering signal distinguishable from background [49]. Similarly, the limit of detection (LOD) was calculated:

$$LOD = Signal_{baseline} + 3 \times SD_{baseline} \quad (3)$$

corresponding to the signal value at a S/N = 3. Further, the concentration and dose at the limit of detection (cLOD/dLOD) were estimated using each regression fit.

As a further measure of sensitivity, the dynamic (log-linear) response range of each fitted dose-response curve was defined as the dose interval over which the response exhibits an exponential increase. This range was extracted from the fitted curves by computing the derivative of the response with respect to log-dose (df(x)/(d log (x))) and identifying the dose interval encompassing 80% of the resulting slope distribution.

The width of this interval was quantified in both log10 and fold-change to describe the magnitude of the dynamic response range.

For direct visual comparison of NF-κB activation response profiles between the two reporter systems, data were normalized to the assay-specific maximal measured response (set to 100%), with all other values expressed as a percentage thereof. This normalization allowed overlay of both dose–response curves on a common relative scale while preserving individual curve shapes and EC_{50}.

For the HEK-pNF-κB-d2EGFP/Neo L2 assay, TNF-α response values were taken from previously published studies and analyzed as reported therein [22]. The original raw data were obtained directly from the corresponding author, ensuring full comparability of data processing between new and previously published datasets. For X-ray experiments using this cell line, response values were generated in the present study as described above.

A detailed summary of replications across all experiments can be found in the Supplementary Excel File (Table S1).

3. Results

3.1. TNF-α-Induced NF-κB Activation

3.1.1. DLR™ Assay: TNF-α Dose Response and Kinetics

Transiently transfected HEK293 cells harboring the pGL4.32 [luc2P/NF-κB-RE/Hygro] reporter plasmid and a pGL4.75 [hRluc/CMV] CMV-driven *Renilla* control plasmid were stimulated with increasing concentrations of recombinant human TNF-α (0–10 ng/mL). Luciferase activity was quantified at five time points (3–24 h) using the DLR™ assay (Figure 2).

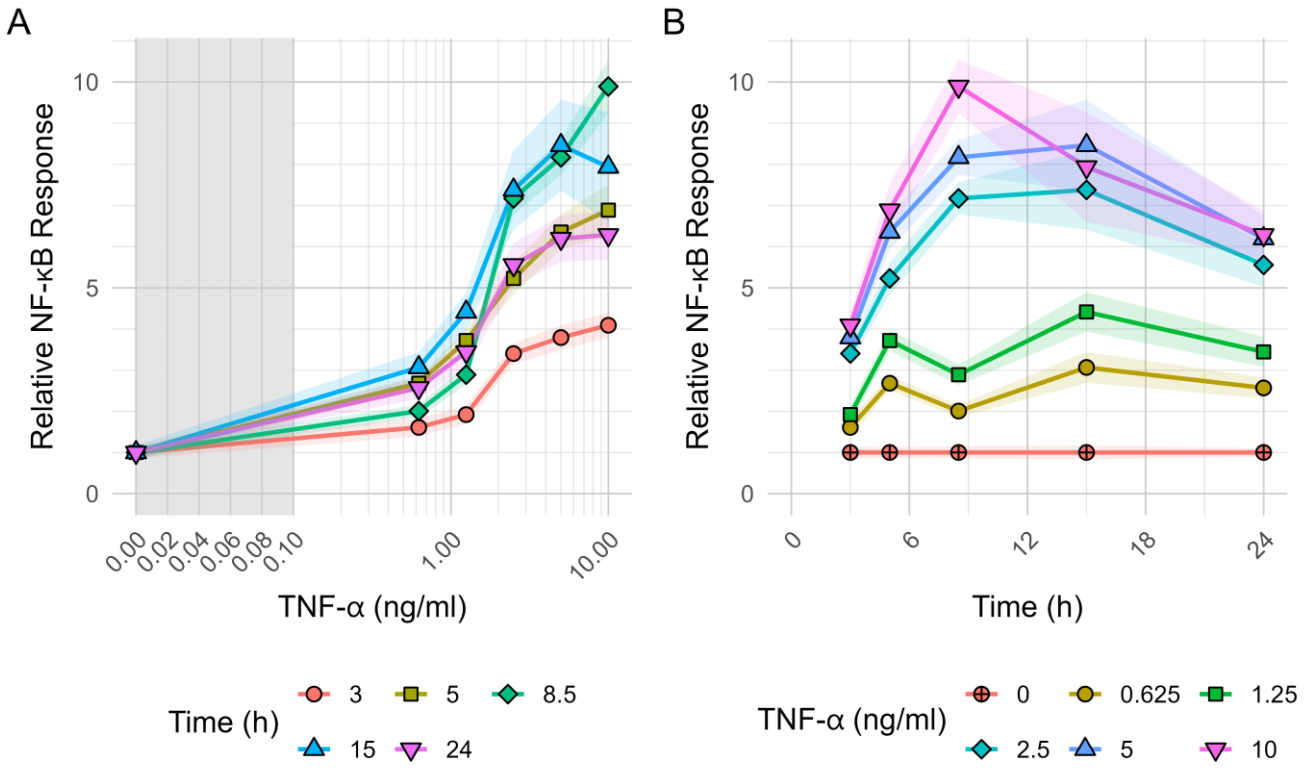


Figure 2. NF-κB activation by TNF-α in HEK293 cells transiently transfected with the DLR™ assay plasmids. (**A**) Dose–response curves for TNF-α stimulation (0–10 ng/mL) at five incubation times (3–24 h). The x-axis is symlog-scaled to visualize full dynamic range. (**B**) Time courses of NF-κB activation at indicated TNF-α concentrations. Data represent baseline-normalized firefly/*Renilla* luciferase ratios (mean fold change). Shaded areas indicate 95% confidence intervals derived from n = 2–7 independent experiments, each with 12–16 replicates.

Activation of the NF-κB-dependent luciferase expression was dose- (Figure 2A) and time-dependent (Figure 2B). Earliest observable induction occurred at 5 h, with a concentration-dependent rise up to 10 ng/mL. Peak responses were reached between 8.5 and 15 h, where the dynamic range extended to ~10-fold above baseline.

At higher TNF-α concentrations (≥2.5 ng/mL), detected response strength declined between 15 h and 24 h, but did not reach baseline values indicating negative signal regulation upon persistent stimulation (Figure 2B).

Overall, the DLR™ assay provided a robust kinetic profile of TNF-α-induced NF-κB activation with clear temporal resolution forming the basis for structured cross-assay comparison with the stably transfected reporter line.

3.1.2. HEK-pNF-κB-d2EGFP/Neo L2 Cell Line: TNF-α Dose Response

The HEK-pNF-κB-d2EGFP/Neo L2 reporter cell line, stably transfected to express destabilized enhanced green fluorescent protein (d2EGFP) under the control of four NF-κB response elements, was originally developed to quantify NF-κB activation via flow cytometry [21]. In a subsequent study, the response of this cell line to stimulation with recombinant human TNF-α was systematically characterized [22].

These cells responded with a clear, dose-dependent activation profile (Figure 3). The baseline without stimulation was a 1 ± 0.74-fold change. Max Response was reached at 5 ng/mL, corresponding to a dynamic range of 16.2.

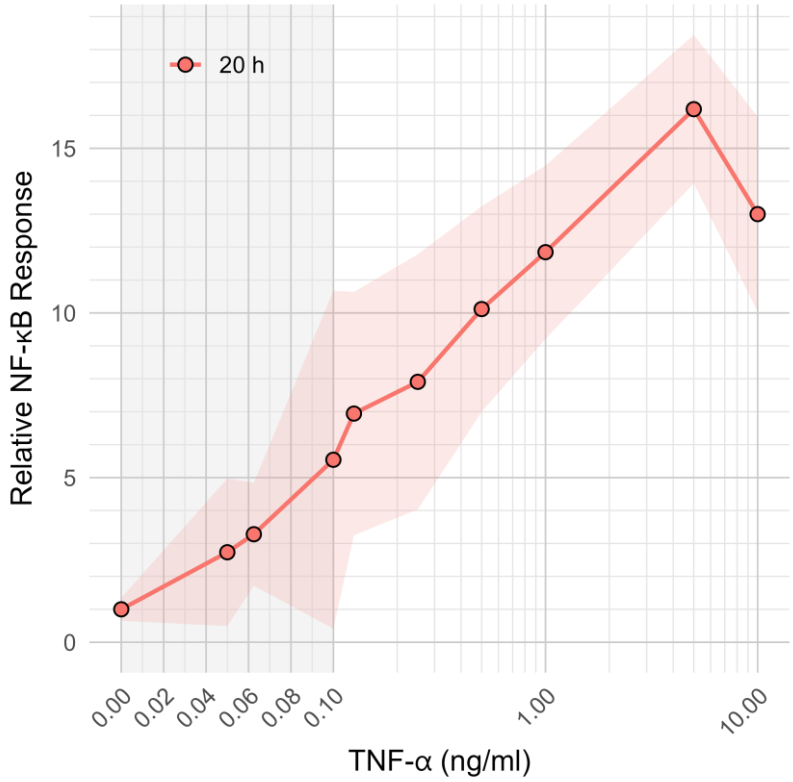


Figure 3. Dose-dependent NF-κB activation in the HEK-pNF-κB-d2EGFP/Neo L2 reporter cell line following 20 h TNF-α stimulation (0–10 ng/mL). NF-κB-driven d2EGFP expression was quantified by flow cytometry and expressed as relative NF-κB response (mean fold change). The shaded area indicates 95% confidence intervals derived from n = 2–10 independent experiments per concentration. The x-axis is symlog-scaled to visualize full dynamic range. Data originate from Hellweg et al. [22].

3.1.3. TNF-α Cross-Assay Comparison of DLR™ Assay and Stable Reporter Cell Line

To enable a direct quantitative comparison of TNF-α–induced NF-κB activation between the transiently transfected DLR™ assay and the stably transfected HEK-pNF-κB-d2EGFP/Neo L2 reporter cell line both datasets were analyzed as described in Section 2.8 (Figure 4). Baseline, LOD, cLOD, dynamic range, concentration at Max Response, EC_{50} values with SE and 95% confidence intervals, Hillslopes, log-linear dynamic range and width as well as S/N at EC50 were determined for each assay (Table 3).

In HEK-pNF-κB-d2EGFP/Neo L2 (Figure 4A), the baseline without TNF-α stimulation was 1 ± 0.74 relative NF-κB response. The highest response was observed at 5 ng/mL TNF-α, corresponding to a dynamic range of 16.2. The four-parameter logistic fit yielded an EC_{50} of 0.31 ± 0.06 ng/mL (95% CI: 0.18–0.45) and a Hillslope of −0.85. The signal-to-noise ratio at the EC_{50} was 10.3.

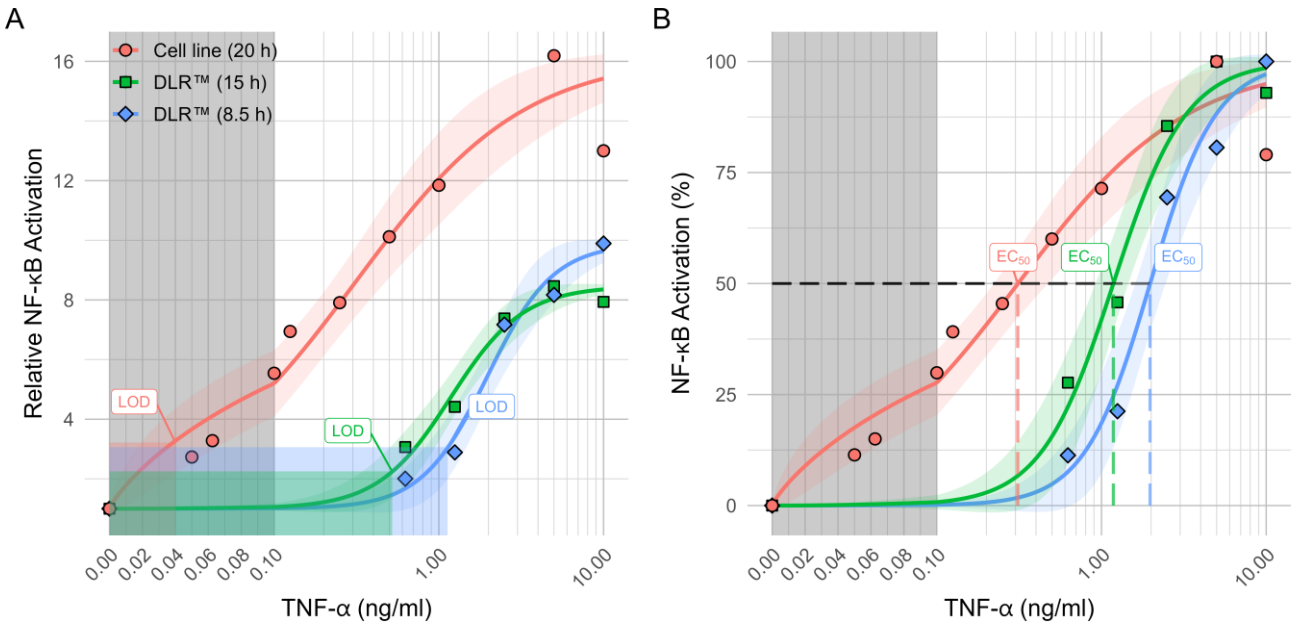


Figure 4. Direct comparison of TNF-α–induced NF-κB activation in the stably transfected HEK-pNF-κB-d2EGFP/Neo L2 cell line and the transiently transfected DLR™ assay. (**A**) Fitted dose–response curves showing relative NF-κB activation in each assay (mean fold change, Cell Line 20 h, DLR™ 15 h, DLR™ 8.5 h). (**B**) Normalized representation, with responses scaled to the assay-specific maximal value (100%) to enable direct comparison of EC_{50} values and curve slope. Data represent mean ± 95% CI (shaded curve areas). The x-axis is symlog-scaled to visualize full dynamic range. Limit of detection (LOD; shaded boxes) and EC_{50} (dotted lines) are indicated corresponding to their respective curve.

Table 3. Parameters of the dose–response curves for NF-κB activation after TNF-α stimulation.

	HEK-pNF-κB-d2EGFP/Neo L2	DLR™ Assay 8.5 h	DLR™ Assay 15 h
Baseline ± SD (fold change) *	1 ± 0.74	1 ± 0.69	1 ± 0.42
LOD (fold change)	3.22	3.06	2.25
cLOD (ng/mL)	0.04	1.13	0.52
Dynamic Range (fold change)	16.19	9.89	8.46
Concentration at Max Response (ng/mL)	5	10	5
EC_{50} ± SE (ng/mL)	0.31 ± 0.06	1.97 ± 0.2	1.18 ± 0.13
EC_{50} 95% CI (low)	0.18	1.34	0.77
EC_{50} 95% CI (high)	0.45	2.61	1.6
Hillslope	−0.85	−2.17	−1.97
Log-linear dynamic range (ng/mL)	0.02–2.49	0.71–4.77	0.39–3.30
Log-linear range width (log10)	2.04	0.83	0.93
Log-linear range width (fold range)	108.98-fold	6.72-fold	8.54-fold
S/N at EC_{50}	10.26	6.49	8.92

* Baseline corresponds to the mean response at 0 ng/mL TNF-α; Limit of detection (LOD) is defined as baseline + 3× standard deviation (SD); the corresponding concentration at LOD (cLOD) is extracted from non-linear regression using a four-parameter logistic (4PL) model; Dynamic Range is the highest observed response value in the dose series; Concentration at Max Response is the concentration at the limit of the dynamic range; EC_{50} values with 95% CI, Hill slopes and log-linear dynamic range and width were obtained from 4PL regression. Signal-to-noise ratio (S/N) was calculated at the EC50 concentration.

In the DLR™ assay (Figure 4A), maximal responses were observed at 5–10 ng/mL TNF-α, with dynamic ranges of 9.9 (8.5 h) and 8.5 (15 h). The fitted EC_{50} decreased from 1.97 ± 0.20 ng/mL (95% CI: 1.34–2.61) at 8.5 h to 1.18 ± 0.13 ng/mL (95% CI: 0.77–1.60) at 15 h, reflecting a time-dependent gain in apparent sensitivity. The corresponding Hill slopes were −2.17 and −1.97, and S/N at EC_{50} were 6.5 and 8.9, respectively. The log-linear dynamic range of HEK-pNF-κB-d2EGFP/Neo L2 has a width of 2.04 orders of magnitude (108.98- fold change, 0.02–2.49 ng/mL), while the dynamic range width of the DLR™ assay lies at 0.83 and 0.93 orders of magnitude for 8.5 and 15 h respectively (8.5 h: 6.72-fold change, 0.71–4.77 ng/mL; 15 h: 8.54-fold change, 0.39–3.30 ng/mL).

LOD for all assays is at ~2–3-fold change in activation. This corresponds to a concentration in HEK-pNF-κB-d2EGFP/Neo L2 of 0.04 ng/mL, while in the DLR™ assay, the signal rises above noise at concentrations of 1.13 and 0.52 ng/mL, for 8.5 and 15 h, respectively. This indicates a higher sensitivity of HEK-pNF-κB-d2EGFP/Neo L2 line.

The normalized dose–response curves illustrate these differences (Figure 4B). While the EC_{50} of the DLR™ assay shifted to a lower value with increasing incubation time, the HEK-pNF-κB-d2EGFP/Neo L2 line consistently showed higher sensitivity, based on a lower EC_{50}, and a broader dynamic range.

3.2. X-Ray-Induced NF-κB Activation

3.2.1. DLR™ Assay X-Ray Dose Response

To quantify X-ray-induced NF-κB activation, HEK293 cells were transiently co-transfected with NF-κB–firefly and CMV–*Renilla* luciferase reporter constructs and exposed to increasing doses of X-rays (0–32 Gy). Reporter activity was determined after 5 h and 8.5 h incubation using the DLR™ assay (Figure 5).

At 5 h, responses increased from baseline (1 ± 0.89) across the analyzed dose range, reaching a dynamic range of 2.61 at 16 Gy. An exploratory measurement at 32 Gy (5 h post-irradiation; $n = 1$) showed a higher response level (4.51-fold change) but was not used for comparison between timepoints.

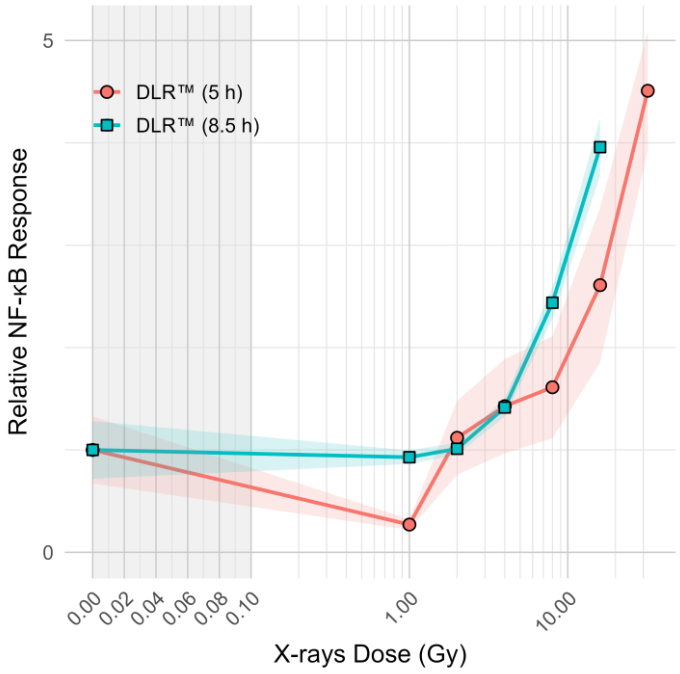


Figure 5. X-ray–induced NF-κB activation in the DLR™ assay. Relative dose–response curves at 5 and 8.5 h post-irradiation. HEK293 cells were irradiated with 0–32 Gy X-rays, and normalized to baseline. Firefly/*Renilla* luciferase ratios were quantified (mean fold change). Shaded areas indicate

95% CI derived from $n = 2–5$ independent experiments per dose, each with 8–16 technical replicates. The x-axis is symlog-scaled to visualize full dynamic range.

At 8.5 h, baseline NF-κB response was a 1 ± 1.08-fold change, and Max Response was reached at 16 Gy, yielding a dynamic range of 3.96.

Overall, both datasets demonstrated monotonic, dose-dependent activation with steeper slopes at higher doses. The dynamic range at 16 Gy is higher for the later time point 8.5 h compared to 5 h—indicating a time dependence in response strength, similar to observation with TNF-α stimulation.

3.2.2. HEK-pNF-κB-d2EGFP/Neo L2 X-Ray Dose Response

The stably transfected NF-κB reporter cell line HEK-pNF-κB-d2EGFP/Neo L2 was exposed to increasing doses of X-rays (0–16 Gy), and NF-κB-dependent EGFP expression was quantified 18 h post-irradiation by flow cytometry (Figure 6).

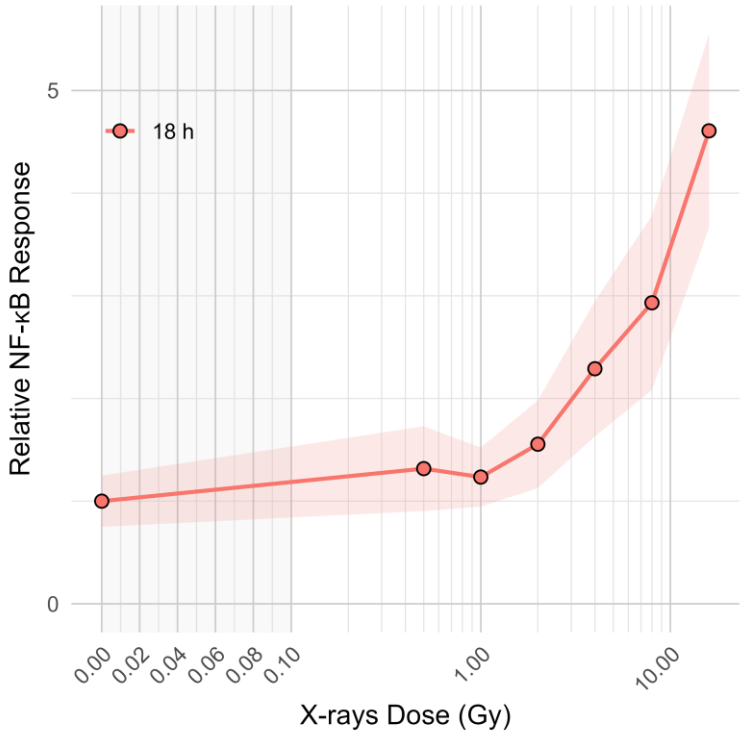


Figure 6. X-ray–induced NF-κB activation in reporter cell line HEK-pNF-κB-d2EGFP/Neo L2. Cells were irradiated with 0–16 Gy X-rays. NF-κB-dependent d2EGFP expression was quantified 18 h post-irradiation by flow cytometry. Data represent mean fold change. The shaded area indicates 95% CI ($n = 5$ independent experiments per dose with 2–3 replicates). The x-axis is symlog-scaled to visualize full dynamic range.

The dose–response curve showed a gradual, monotonic increase in NF-κB activation with increasing radiation dose. Baseline response was a 1 ± 0.48-fold change. Max Response was observed at 16 Gy, corresponding to a dynamic range of 4.61.

Overall, NF-κB activation increased dose-dependently in the HEK-pNF-κB-d2EGFP/Neo L2 reporter line after X-ray exposure.

3.2.3. X-Ray Cross-Assay Comparison of DLR™ Assay and Stable Reporter Cell Line

To directly compare assay performance, NF-κB activation data from the transiently transfected DLR™ assay and stably transfected HEK-pNF-κB-d2EGFP/Neo L2 line were evaluated following X-ray irradiation. For the DLR™ assay, mean responses at 8.5 h post-

irradiation were obtained from four biological replicates per dose. For the HEK-pNF-κB-d2EGFP/Neo L2 cell line, measurements were taken at 18 h post-irradiation from five biological replicates.

Nonlinear regression with a four-parameter logistic (4PL) model was applied to visualize curve differences (Figure 7). Curve fits were used to determine baseline activity, limit of detection and its corresponding dose, dynamic range and concentration at Max Response, ED_{50} values with 95% confidence intervals, Hillslopes, log-linear dynamic range width and S/N at ED_{50} (Table 4).

Table 4. Parameters of the dose–response curves for NF-κB activation in the HEK-pNF-κB-d2EGFP/Neo L2 reporter cell line and the transient DLR™ assay following X-ray exposure.

Parameter	HEK-pNF-κB-d2EGFP/Neo L2	DLR™ Assay 8.5 h
Baseline ± SD (fold change) *	1 ± 0.48	1 ± 1.08
LOD (fold change)	2.43	4.23
dLOD (Gy)	4.57	>16 Gy
Dynamic Range (fold change)	4.61	3.96
Dose at Max response (Gy)	16	16
ED_{50} ± SE (Gy)	5.77 ± 0.87	7.82 ± 0.49
ED_{50} 95% CI (low)	3.36	6.26
ED_{50} 95% CI (high)	8.18	9.37
Hill slope	−1.81	−3.65
Log-linear dynamic range (Gy)	1.59–11.34	4.22–12.12
Log-linear range width (log10)	0.85	0.46
Log-linear range width (fold range)	7.11-fold	2.87-fold
S/N at ED_{50}	3.79	1.37

* Baseline corresponds to the mean response at 0 Gy; Limit of detection (LOD) is defined as baseline + 3× standard deviation (SD); the corresponding dose at LOD (dLOD) is extracted from non-linear regression using a four-parameter logistic (4PL) model; for the DLR™ assay, dLOD exceeds the highest tested irradiation dose and is therefore indicated as greater than the maximum experimental range; Dynamic range is the highest observed response value in the dose series; Concentration at Max Response is the dose at the limit of the dynamic range; ED_{50} values with 95% confidence intervals, Hillslopes and log-linear dynamic range and width were obtained from 4PL regression. Signal-to-noise ratio (S/N) was calculated at ED_{50}. Data for the HEK-pNF-κB-d2EGFP/Neo L2 cell line is based on $n = 5$ biological replicates; DLR™ data are based on $n = 5$ biological replicates.

For the DLR™ assay 8.5 h after exposure, maximal fold change response at 16 Gy was 3.96, with an ED_{50} of 7.82 Gy (95% CI: 6.26–9.37), and a Hill slope of −3.65. The signal-to-noise ratio at ED_{50} was 1.37.

In contrast, the HEK-pNF-κB-d2EGFP/Neo L2 cell line showed a maximal induction of 4.61-fold change at 16 Gy, with an ED_{50} of 5.77 Gy (95% CI: 3.36–8.18) and a Hill slope of −1.81. The signal-to-noise ratio at the ED_{50} was 3.79.

The limit of detection (Figure 7A) for the HEK-pNF-κB-d2EGFP/Neo L2 cell line is at 2.43-fold change, corresponding to a dose of 4.57 Gy. For the DLR™ assay LOD is higher than its dynamic range, so a dose cannot be extracted from the 4PL fit.

The log-linear dynamic range of HEK-pNF-κB-d2EGFP/Neo L2 has a width of 0.85 orders of magnitude (7.11-fold change, 1.59–11.34 Gy), while the dynamic range width of the DLR™ assay encompasses 0.46 orders of magnitude (2.87-fold change, 4.22–12.12 Gy). This indicates a higher sensitivity of the reporter cell line.

In comparison, while with the DLR™ assay, relative luminescence does not rise above noise level at the 8.5 h time point, an observable increase in relative NF-κB activation was

detected at a dose of 4 Gy with the HEK-pNF-κB-d2EGFP/Neo L2 cell line, denoting a higher detection sensitivity.

Normalized dose–response curves from both assays were fitted with the 4PL model and are shown in Figure 7B. The ED_{50} values of the HEK-pNF-κB-d2EGFP/Neo L2 cell line was lower for the DLR™ assay, indicating greater sensitivity (Figure 7B).

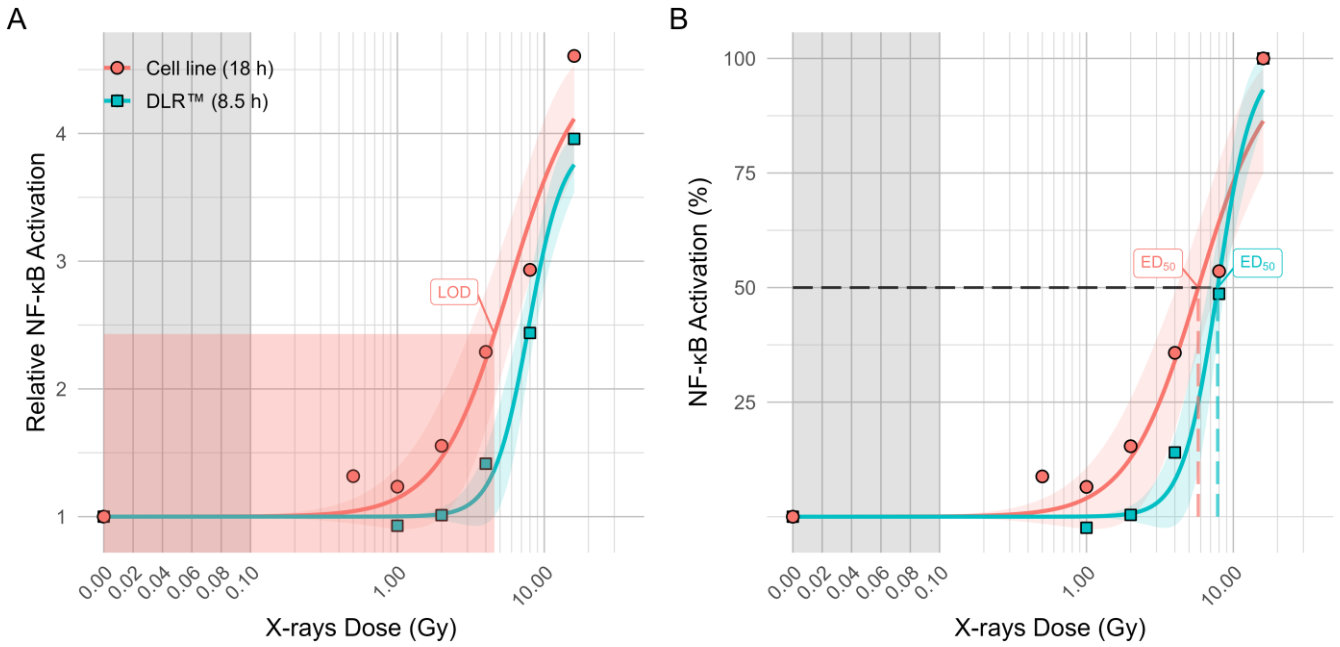


Figure 7. Normalized X-ray dose–response curves for NF-κB activation in the DLR™ assay (8.5 h post-irradiation) and the HEK-pNF-κB-d2EGFP/Neo L2 cell line (18 h post-irradiation). (**A**) Fitted dose–response curves showing relative NF-κB activation in each assay (mean fold change, Cell line 18 h, DLR™ 8.5 h). (**B**) Normalized representation, with responses scaled to the assay-specific maximal value (100%) to enable direct comparison of ED_{50} values and curve slope. Data represent mean ± 95% CI (shaded curve area). The x-axis is symlog-scaled to visualize the full dynamic range. Limit of detection (LOD) is given for the HEK-pNF-κB-d2EGFP/Neo L2 cell line (shaded box), ED_{50} is marked for the respective curves (dotted lines).

4. Discussion

In this study, we compared two widely used reporter systems for quantifying NF-κB activation: the transient DLR™ assay in HEK293 cells and the stably transfected HEK-pNF-κB-d2EGFP/Neo L2 cell line. Both systems were tested under harmonized conditions using recombinant human TNF-α and X-rays as representative stimuli. The comparison was based on several critical performance parameters, including sensitivity (EC_{50}/ ED_{50}, LOD, log-linear dynamic range), dynamic assay range, signal-to-noise ratio (S/N), and scalability. These results provide important insights into the strengths and limitations of each system, offering clear guidance for assay selection in various experimental contexts. Due to the fundamentally different measurement principles and signal kinetics of luminescence- and fluorescence-based reporters, the present comparison is not intended as a universal method-level evaluation, but rather as a pragmatic, use-case-driven assessment of two specific NF-κB reporter implementations under defined experimental readout endpoints.

HEK-pNF-κB-d2EGFP/Neo L2 show higher sensitivity and dynamic range after TNF-α treatment

One of the primary performance parameters we assessed was sensitivity, measured as EC_{50} indicating the concentration or dose of a stimulus required to produce half of the maximal response, as well as LOD and its corresponding concentration/dose (cLOD/dLOD) and the log-linear dynamic range.

The limit of detection, as baseline + 3× its standard deviation, marks the assay's signal range that can be considered noise, correlating to an S/N < 3 [49]. In the case of TNF-α stimulation, the HEK-pNF-κB-d2EGFP/Neo L2 cell line exhibited a distinctly lower cLOD than the DLR™ assay, indicating detection of NF-κB activation at much lower concentrations of TNF-α. Within the specific assay configuration tested here, this makes the HEK-pNF-κB-d2EGFP/Neo L2 cell line a more sensitive tool for applications requiring the detection of low-level activation.

Inspection of the TNF-α dose–response curves further indicates that NF-κB activation in the HEK-pNF-κB-d2EGFP/Neo L2 cell line becomes detectable at substantially lower cytokine concentrations than in the transient DLR™ assay. In the low-concentration regime, the stable reporter cell line exhibits a gradual increase in signal, whereas the DLR™ assay shows a steeper response that becomes apparent only at higher TNF-α concentrations. This behavior is consistent with the lower cLOD values observed for the stable reporter system and reflects assay-specific sensitivity characteristics rather than a strict biological activation threshold. This interpretation is further supported by the broader log-linear response range observed for the HEK-pNF-κB-d2EGFP/Neo L2 cell line under the tested conditions.

Furthermore, with its larger dynamic range, HEK-pNF-κB-d2EGFP/Neo L2 can be assumed to provide higher precision under the defined experimental conditions.

Among DLR™ assay time points, the highest response is reached at different concentrations. While the dynamic range was lower at 15 h compared to 8.5 h, this level of response is at 50% of the concentration at 8.5 h. This suggests that the readout time should be optimized within each assay system for the respective cell and stimulus type.

Response kinetics reflect assay-specific reporter turnover and NF-κB signaling dynamics after TNF-α stimulation

The two reporter systems compared in this study differ in their molecular design and readout principles [18,21], so consideration of temporal dynamics is important for use of these NF-κB reporter assays. They were analyzed at different post-stimulation time points to reflect their assay-specific response kinetics and signal maturation characteristics. Firefly luciferase reporters, including the destabilized form (luc2P) used in this study, provide a rapid and transient readout of NF-κB activation, with peak signals observed within a few hours after stimulation, as shown in Figure 2. Luciferase reporter signal reportedly started to decline in HeLa cells between 8 and 10 h post-stimulation with TNF-α [50]. A similar trend, with decline-onset between 8 and 15 h post-stimulation was observed in the luc2P-utilizing DLR™ assay (Figure 2B). This time-dependent attenuation of the signal is a well-established phenomenon in the DLR™ assay and may limit its ability to capture prolonged or sustained activation in certain experimental contexts [51] but may allow detection of oscillating signaling pathway activation. The decline of the DLR™ reporter signal at later time points is primarily attributable to assay-specific reporter turnover characteristics. The destabilized luc2P is a rapidly turned-over enzyme with a short functional half-life, leading to transient signal profiles following pathway activation [18]. Its half-life is reported to be ~0.8 h in T-47D cells [52], shorter compared to its wildtype at 2 to 3 h in HEK293T or HepG2 respectively [53,54].

While NF-κB signaling is known to be regulated by negative feedback mechanisms, including IκBα resynthesis and nuclear–cytoplasmic shuttling occurring within the first hours after stimulation, the temporal signal behavior observed here is more parsimoniously explained by differences in reporter stability and readout kinetics rather than a

direct reflection of NF-κB feedback dynamics [51,55,56]. Accordingly, the DLR™ assay is well suited to capture early pathway activation events but is less suitable for assessing sustained or long-term NF-κB activity [55].

In contrast, the destabilized EGFP reporter used in the HEK-pNF-κB-d2EGFP/Neo L2 cell line is designed to reduce intracellular persistence compared to conventional EGFP [56]. The cell line exhibits delayed signal accumulation and reaches stable, consistent response levels at later time points, which are maintained over several days of treatment, as previously characterized [21]. The fluorescence signal of d2EGFP was described to have a half-life of 2 h in CHO K1 Tet-off cells [56] and 5.3 h in HEK cells after cycloheximide treatment [57]. This indicates that the cell line is less suitable for detecting transient or oscillatory activation patterns, as the accumulation and slower turnover of d2EGFP tend to mask short-term dynamics. However, its stable and reproducible signal makes it advantageous for experiments that require quantification of sustained NF-κB activation or long-term endpoint measurements.

Stronger differences in signal kinetics of green fluorescence from d2EGFP compared to luminescence from the luciferase-catalyzed reaction could therefore be attributed to the different half-lives, to the maturation of the reporter protein and to the fact that the d2EGFP fluorescence signal depends on the accumulated and correctly folded d2EGFP, while the luminescence signal depends on the luciferin reaction that is catalyzed by the luciferase amount that is present at the time of reaction [58]. Therefore, we focused on the functional reporter response kinetics, as reflected by the time-dependent signal development following pathway activation, which integrates maturation, half-life and readout characteristics. The selected detection time points were based on previously published characterizations of the respective reporter systems and were chosen to capture the dynamic response window of each assay rather than to directly match absolute incubation times. Accordingly, differences in temporal signal behavior cannot be attributed to a single parameter such as protein half-life alone.

Consequently, differences in the temporal signal profiles observed between the two systems should be interpreted in the context of their distinct reporter turnover characteristics and assay-specific response kinetics, rather than as direct measures of NF-κB signaling dynamics alone.

Signal origins and promoter architecture determine reporter signal accessibility

The difference in signal accessibility originates from the different signal origins. Luciferases are small proteins formed in short amounts of time, reaching peak signal earlier than fluorescent proteins [52,59], while EGFP and variants such as d2EGFP require longer periods of maturation and accumulation, leading to peak signal ~20–24 h after induction that can be sustained in HEK cells for several hours in case of d2EGFP and several days in case of EGFP [57]. This marks a trade-off between temporal resolution and precision between the different reporters, as observed in this study (Figure 4A).

Beyond kinetic regulation by feedback mechanisms and reporter turnover, differences in promoter architecture may also underlie the distinct activation profiles observed between the two systems. The pGL4.32 construct used in the DLR™ assay contains five tandem copies of the NF-κB response element upstream of a minimal TATA promoter, which provide strong inducibility but can also influence the kinetics and saturation behavior of the reporter [47,60]. In contrast, the promoter configuration of the HEK-pNF-κB-d2EGFP/Neo L2 cell line is based on an earlier design with distinct spacing and regulatory sequences, which may partly explain its higher sensitivity and more stable activation profile at intermediate TNF-α concentrations [21].

Differences in promoter architecture, including the number and arrangement of NF-κB response elements, have been shown to influence transcriptional output and activation thresholds in NF-κB–dependent reporter systems [61,62]. Previous studies demonstrated

that variations in response element copy number can modulate signal amplitude and sensitivity, but do not act as isolated determinants of pathway activation strength, as transcriptional output is additionally shaped by promoter context, chromatin accessibility and reporter design [63,64].

Accordingly, while the difference in NF-κB response element number between the two reporter systems used in this study may contribute to the observed differences in activation profiles, it is unlikely to fully account for the pronounced differences in sensitivity and dynamic range. Instead, the results reflect the combined effects of promoter architecture, reporter turnover characteristics and assay-specific readout principles.

NF-κB activation in response X-rays exposure challenging to detect at low doses, with limited precision at high doses

After X-ray exposure, NF-κB activation increased dose-dependently in both the DLR™ assay and the HEK-pNF-κB-d2EGFP/Neo L2 cell line, with the cell line exhibiting higher sensitivity within the tested assay configuration, similar to TNF-α stimulation. LOD in HEK-pNF-κB-d2EGFP/Neo L2 is overcome at a dose of 4.57 Gy with a 2.43-fold NF-κB activation. On the other hand, the detection limit of the DLR™ assay at 8.5 h is higher than its dynamic range (LOD 4.23-fold vs. dynamic range 3.96-fold). This implies that NF-κB responses elicited by X-ray exposure are difficult to assess with either assay, especially at lower doses, which is further underlined by S/N at ED_{50} of both assays, with HEK-pNF-κB-d2EGFP/Neo L2 at 3.79 and DLR™ assay < 2, as well as the width of their log-linear dynamic ranges, which is 0.85 vs. 0.46 orders of magnitude for HEK-pNF-κB-d2EGFP/Neo L2 and DLR™ assay, respectively. It should be noted that the signal-to-noise ratio (S/N) reported here is calculated based on the standard deviation of the baseline signal, whereas the 95% confidence intervals shown in Figure 7 reflect the uncertainty of the non-linear regression fit and do not represent experimental noise at ED_{50}.

The HEK-pNF-κB-d2EGFP/Neo L2 system further reinforces its higher signal clarity within this specific assay configuration, particularly in terms of precision and resolution at higher doses. Other radiation qualities such as high LET heavy ions may induce NF-κB to a stronger degree, allowing this assay to be suitable even below 4 Gy [22,23,65,66].

An exploratory high dose value (32 Gy) for the DLR™ assay at 5 h elevates the dynamic range of this assay to 4.5-fold. This level is comparable with the HEK-pNF-κB-d2EGFP/Neo L2 cell line (dynamic range = 4.61-fold), albeit at twice the dose. At 16 Gy, the 8.5 h time point of the DLR™ assay achieves a 4.05-fold increase over baseline, compared with 2.61-fold at 5 h. At the same dose the stable cell line shows a slightly better capacity within the tested readout conditions to detect X-ray-induced NF-κB activation.

High versatility of the DLR™ assay is limited by setup complexity and costs

The DLR™ assay would be especially useful in rapid screening or large-scale kinetic studies. with fast signal production and turnover that can be processed in 96-well or higher-density formats. Its integrated viability correction using ratiometric Firefly/*Renilla* normalization minimizes background noise and signal interference, which is crucial in assays where high-throughput and automation are the primary objectives [16]. The DLR™ assay additionally offers the flexibility of being transiently transfected into any desired cell line, allowing adaptation to various experimental settings including a wide range of cell types. Thus, it becomes feasible to explore more specialized cell types such as SH-SY5Y neuroblastoma cells, commonly used in neurobiological research due to their ability to differentiate into neuron-like cells and their relevance in neuroinflammation and neurodegenerative diseases [67].

As with all transiently transfected reporter assays, the performance of the DLR™ system is influenced by transfection efficiency. However, the use of an internal *Renilla* luciferase control for well-by-well normalization represents an integral component of the

DLR™ assay design and effectively compensates for variability in transfection efficiency and cell number within individual experiments [68,69].

This flexibility in cell line selection gives the DLR™ assay a significant edge when specific cellular contexts need to be examined, at the cost of sensitivity and precision in the present assay configuration. Additionally, this assay has a higher setup complexity, involving the use of a dual-color luminescence plate read with an integrated heating unit and liquid dispenser, as well as reagents consumables that increase cost considerations.

High sensitivity and ease of assay implementation of HEK-pNF-κB-d2EGFP/Neo L2 cell line limited by need for additional viability control, signal dynamics and inflexible cell type choice

HEK-pNF-κB-d2EGFP/Neo L2 cell line offers substantial sensitivity and precision within the tested experimental framework, particularly valuable for toxicity and radiation response profiling, and studies requiring precise quantification of low-level activation. Flow cytometric assessment at the single-cell level promotes use of this reporter in mechanistic studies or analysis of cellular heterogeneity. It provides granular insights at the population level that can be expanded with implementation of large immunofluorescent marker panels, cell cycle analysis, or sorting for downstream applications such as single-cell transcriptomics. While no dedicated viability dye was included in the present flow cytometry experiments, the use of live/dead discrimination dyes would represent a valuable additional control to ensure that reporter signals originate exclusively from viable cells. Accordingly, the lack of integrated viability control represents a limitation of the current setup, which could be ameliorated by implementing comparable cell systems to monitor viability, such as HEK-pEGFP-N1, a CMV-promoter–driven reporter cell line with constitutive EGFP expression [70] or a red fluorescent reporter cell line with constitutive tdTomato expression [71]. Addition of a viability dye prior to fixation can be used to gate for viable cells and assess NF-κB response signal in this population.

In the present study, reporter activation in the HEK-pNF-κB-d2EGFP/Neo L2 cell line was quantified based on the percentage of EGFP-positive cells, which provides a robust and reproducible metric for NF-κB activation at the population level [72]. Alternative quantification strategies, such as combining the fraction of EGFP-positive cells with mean fluorescence intensity (MFI), may capture additional information on expression amplitude per cell and could be informative for specific mechanistic questions [73]. In addition, fluorescence-based NF-κB reporters can be read out using either flow cytometry or fluorescence plate readers. The use of plate readers for fluorescence signals necessitates consideration of autofluorescence from media and cell cultures plates, as well as absolute fluorescence levels of the fluorophore. The low absolute level d2EGFP-fluorescenceexcludes plate reader quantification of d2EGFP expressed by cells in 96-well-plates formats, while EGFP could be quantified [21]. Plate reader-based approaches may facilitate higher-throughput measurements and closer alignment with luminescence-based assay formats, while flow cytometry provides single-cell resolution and enables assessment of cellular heterogeneity, multiparametric phenotyping, and cell sorting [74]. The choice of readout platform therefore represents a trade-off between throughput, accessibility, and analytical depth, depending on the experimental objective.

Even though this assay has a low-cost factor and setup complexity, its key downsides are model inflexibility, being bound to HEK293 cells, and slow signal onset and accumulation, leading to longer acquisition times. In principle, integration copy number may influence basal reporter activity, the assay performance discussed here reflects the empirically selected clone behavior reported for L2 under standard culture conditions.

Assay choice determined by experimental endpoints and study considerations

Both assays offer distinct advantages depending on the experimental needs. Both assays are well suited for high-throughput applications and easily scalable.

When choosing between these two assays, the decision largely depends on the experimental requirements and constraints. For large-scale screening, especially in contexts requiring rapid compound testing or kinetic titrations, the DLR™ assay is the preferred choice due to its detection speed, and ability to be integrated with automation systems. The HEK-pNF-κB-d2EGFP/Neo L2 cell line, however, is better suited for experiments that require high precision or downstream applications, such as those involving mechanistic insights, radiation biology, or dose–response analysis at low levels of activation.

Moreover, for spaceflight-related studies, particularly those involving radiation exposure in combination with microgravity simulations or real space conditions, technical integration becomes a decisive factor. The DLR™ assay, with its requirement for dual-reagent injection and immediate luminescence readout, significantly increases hardware complexity, making it less suitable for autonomous payloads where minimalistic setups are often preferred. In contrast, the stable HEK-pNF-κB-d2EGFP/Neo L2 reporter cell line offers a few major advantages: it needs little preparation or upkeep for consistent signal production and can be chemically fixed at the desired endpoint, this simplifies payload architectures and removes the need for continuous monitoring or sophisticated luminescence detection systems during the mission. This capability to fix cells at their peak activation without the need for complex instrumentation allows for the use of more straightforward, modular fixation systems such as syringe-based modules [75,76], making it an excellent choice for biological spaceflight experiments.

The ability to chemically preserve NF-κB activity at endpoint is particularly relevant when considering the environmental challenges of space missions, where conditions such as microgravity and radiation can severely affect cellular responses. Maintaining the integrity of NF-κB readouts during pre- and post-exposure handling requires strictly controlled environmental conditions. Even minor fluctuations in temperature during transport or in-flight handling can significantly affect pathway activity. Heat shock has been shown to attenuate TNF-α-induced NF-κB responsiveness, with delayed recovery times. Moreover, heat shock independently activates NF-κB and other stress responses such as heat-shock protein expression, as observed in macrophages [77,78]. These findings underline the importance of transport solutions that can ensure stable culture conditions, such as purpose-built transport incubators for biological spaceflight payloads [79].

Furthermore, considering the complexity of autonomous systems in space, the established, stably transfected reporter cell lines present a cost-effective and technically feasible option for radiation experiments in low-Earth orbit or long-duration missions, where simplicity and reliability are paramount. By removing the need for real-time analysis equipment and enabling post-mission analysis via fixed samples, this method aligns well with the operational constraints of space biology experiments [75].

Conclusion and future directions

Despite the strengths of both assays, there are limitations to consider. The increased difficulty for both assays to assess low-dose X-ray-mediated responses indicates that some experimental conditions or endpoints need reporter systems with improved sensitivity. In this context, it should be noted that newer luciferase-based reporter formats with substantially increased signal output, such as NanoLuc, have become available and may further alter assay performance characteristics [80]. Compared to classical firefly luciferase, these systems provide markedly higher intrinsic brightness and can be measured using glow-type luminescence readouts without the need for reagent injection, thereby simplifying hardware requirements [81]. The use of such alternative luciferase formats could therefore lead to different sensitivity, dynamic range, and comparability outcomes when contrasted with fluorescence-based NF-κB reporter cell lines [72,82].

In addition, stably transfected HEK293 reporter cell lines expressing luciferase under the control of NF-κB–dependent promoters have been described and represent another

widely used NF-κB reporter configuration [72]. Such stable luciferase-based reporters combine fixed genomic integration with enzymatic luminescence readouts and may therefore exhibit performance characteristics distinct from both transient dual-luciferase assays and fluorescence-based reporter cell lines [83,84]. A cross-assay between transient and stable luciferase-based NF-κB reporters would address a different experimental question and was beyond the scope of the present study. Nevertheless, the availability of these alternative reporter designs further emphasizes that NF-κB reporter performance is highly implementation-dependent and that comparative outcomes strongly depend on the specific reporter architecture, readout principle, and experimental context.

Along similar lines, improved sensitivity in fluorescence-based systems could be achieved by implementing brighter fluorophores such as mNeonGreen or Clover [85,86] or DDtdTomato combined with a stabilizer which allowed detection of NF-κB activation by one energetic argon ion traversing the cell nucleus [87]. Another point of consideration is the unit difference in assay readout between the two systems (relative luminescence units–RLU vs. % EGFP$^{(+)}$ cells), which necessitates careful normalization for valid comparison. Variability in intra-plate signal-to-noise ratios and inter-experiment reproducibility should be further assessed to better understand assay consistency across a wider range of conditions.

Additionally, variability in intra-plate S/N and inter-experiment reproducibility should be further assessed to understand assay consistency across a wider range of conditions. Future developments of reporter-based NF-κB assays may therefore benefit from integrated normalization and control strategies, including constitutively expressed reference reporters and the use of viability dyes during flow cytometric analysis, particularly under stress-inducing conditions such as irradiation. In addition, alternative reporter vector architectures, such as single-vector dual-reporter formats, could further reduce variability associated with transient co-transfection.

Differences in temporal resolution of signal production and retention shape considerations for assay design. While transient reporters allow flexibility in choice regarding host system, transfection vector and luciferase/fluorescent proteins, they inherently suffer to some degree loss of transfection efficiency and intra-assay signal consistency. This is not the case for stably transfected reporters, but optimization and implementation of such a system is costly and time-consuming [57,88,89].

Future directions include the use of next-generation reporter lines, with rapid-turnover fluorophores or degron/ProteoTuner-based constructs, which could improve precision and scalability while maintaining single-cell resolution [71,87]. Furthermore, optimizing dose-time matrices across both assays and exploring high-LET radiation types would help resolve subtle differences in potency and response kinetics in radiation studies [90,91].

In summary, both the DLR™ assay and the HEK-pNF-κB-d2EGFP/Neo L2 cell line demonstrates comparable potency within the experimental framework investigated here for detecting NF-κB activation in response to TNF-α and X-rays. The DLR™ assay offers advantages in high-throughput screening, automation, and rapid readout, while the HEK-pNF-κB-d2EGFP/Neo L2 cell line provides greater precision, single-cell resolution, and higher sensitivity within the specific assay implementation tested in this study. The choice between these assays depends on the experimental context, with the DLR™ assay being optimal for large-scale screenings and HEK-pNF-κB-d2EGFP/Neo L2 for mechanistic studies and experiments requiring precise quantification at low activation levels (Table 5).

Table 5. Characteristics and performance parameters of the Dual-Luciferase® Reporter (DLR™) assay and the stably transfected HEK-pNF-κB-d2EGFP/Neo L2 reporter cell line.

Parameter	DLR™ Assay	HEK-pNF-κB-d2EGFP/Neo L2	Reference
Number of NF-κB response elements	5	4	[21,47]
Versatility: cell types	High transiently applicable to any transfectable cell line	Low restricted to HEK293 background	[18,21]
Scalability	High 96 well high-throughput capability	High 96 well high-throughput capability	Sections 2.3 and 2.4, Discussion Section 4 (this study)
Setup complexity	High requires transient transfection, reagent addition, and dual-injector readout	Low ready-to-use stable line, no transfection required	Sections 2.3 and 2.4 (this study)
Infrastructure	Luminescence microplate reader with dual injector, heating and shaking	Flow cytometer/Fluorescence microscope	Sections 2.3 and 2.7 (this study)
Cost	High plasmids, transfection reagent, substrates	Low standard media and G418 selection only	Discussion Section 4 (this study)
Sensitivity—canonical NF-κB activation	Moderate cLOD: 0.52 ng/mL (15 h) EC_{50}: 1.18 ± 0.13 ng/mL (15 h) Log-linear range width: 8.54-fold (15 h)	High cLOD: 0.04 ng/mL EC_{50}: 0.31 ± 0.06 Log-linear range width: 108.98-fold	Discussion Section 4 and Table 3–4 (this study)
Sensitivity—genotoxic stress-induced NF-κB activation	Low dLOD: not defined in test range ED_{50}: 7.82 ± 0.49 Gy Log-linear range width: 2.87-fold	Moderate dLOD: 4.57 Gy X-rays ED_{50}: 5.77 ± 0.87 Gy Log-linear range width: 7.11-fold	Discussion Section 4 and Tables 3 and 4 (this study)
Reporter protein–Maturation time	Minutes luciferase active shortly after translation	~20 h d2EGFP requires folding and chromophore maturation	[21,52]
Reporter protein–Accumulation time	3–15 h to peak luminescence	18–24 h to peak fluorescence	Figures 2 and 3 (this study)
Reporter protein–Half-life	~0.8 h (luc2P)	2–5.3 h (d2EGFP)	[52,56,57]
Reporter protein–Half-life modulation	By destabilization tags (luc2P); alternative ProteoTuner possible	Via degron/ProteoTuner systems (e.g., DD-tdTomato + Shield-1)	[87]
Substrate requirement	Requires luciferin and Stop & Glo® reagents	None—fluorescence depends only on oxygen availability	[18,21]
Single cell information	No—bulk luminescence measurement	Yes—fluorescence quantified by flow cytometry	Section 2.7 (this study)
Integration compatibility with other assays	Not possible– cells are lysed for measurement	Fully compatible– can be combined with other fluorescent or viability markers	[21,71]

Supplementary Materials: The following supporting information can be downloaded at: https://www.mdpi.com/article/10.3390/mps9060164/s1, Table S1: Assay replicates.

Author Contributions: Conceptualization, C.B.-K., S.F. and S.D.; methodology, S.F., S.D., C.B.-K. and C.E.H.; software, S.F., S.D. and C.B.-K.; validation, S.F., S.D., C.B.-K. and C.E.H.; formal analysis, S.F. and S.D.; investigation, S.F., S.D., B.H., C.B.-K. and C.E.H.; resources, C.B.-K. and C.E.H.; data curation, S.F. and S.D.; writing—original draft preparation, S.F. and S.D.; writing—review and editing, S.F., S.D., B.H. and C.E.H.; visualization, S.F. and S.D.; supervision, C.B.-K. and C.E.H.; project

administration, C.B.-K. and C.E.H.; funding acquisition, C.B.-K. and C.E.H. All authors have read and agreed to the published version of the manuscript.

Funding: This research received no external funding.

Institutional Review Board Statement: Not applicable.

Informed Consent Statement: Not applicable.

Data Availability Statement: The data that support the findings of this study are available from the corresponding author upon reasonable request.

Acknowledgments: The authors thank their colleagues from the Cellular Biodiagnostics group of the Department of Radiation Biology at the Institute of Aerospace Medicine (DLR) for their support and constructive discussions throughout this work. Figure 1 was created with BioRender.com.

Conflicts of Interest: The authors declare no conflicts of interest.

Abbreviations

The following abbreviations are used in this manuscript:

4PL	Four-parameter logistic model
α-MEM	Minimum Essential Media Alpha (Eagle)
bp	Base pairs
CI	Confidence interval
cLOD	Concentration at Limit of Detection
CMV	Cytomegalovirus promoter
d2EGFP	Destabilized Enhanced Green Fluorescent Protein
DLR™	Dual-Luciferase® Reporter Assay
dLOD	Dose at Limit of Detection
DNA	Deoxyribonucleic acid
EC_{50}	Half-maximal effective concentration
ED_{50}	Half-maximal effective dose
FBS	Fetal bovine serum
FSC	Forward scatter
Gy	Gray (unit of absorbed radiation dose)
HEK293	Human embryonic kidney 293 cell line
LAR II	Luciferase Assay Reagent II
LET	Linear energy transfer
LOD	Limit of detection
Max Response	Maximal measured response within tested range
NAMs	New approach methodologies
NF-κB	Nuclear factor kappa-light-chain-enhancer of activated B cells
PBS	Phosphate-buffered saline
PMA	Phorbol 12-myristate 13-acetate
R	Statistical computing environment (R Foundation)
RLU	Relative luminescence units
S/N	Signal-to-noise ratio
SD	Standard deviation
SE	Standard error
SV40	Simian Virus 40 (enhancer/promoter region)
TNF-α	Tumor necrosis factor alpha
X-rays	Ionizing radiation generated by an X-ray tube

References

1. Barnabei, L.; Laplantine, E.; Mbongo, W.; Rieux-Laucat, F.; Weil, R. NF-κB: At the borders of autoimmunity and inflammation. *Front. Immunol.* **2021**, *12*, 716469.
2. Gómez-Chávez, F.; Correa, D.; Navarrete-Meneses, P.; Cancino-Diaz, J.C.; Cancino-Diaz, M.E.; Rodríguez-Martínez, S. NF-κB and its regulators during pregnancy. *Front. Immunol.* **2021**, *12*, 679106.
3. Mussbacher, M.; Derler, M.; Basílio, J.; Schmid, J.A. NF-κB in monocytes and macrophages–an inflammatory master regulator in multitalented immune cells. *Front. Immunol.* **2023**, *14*, 1134661.
4. Biswas, R.; Bagchi, A. NFkB pathway and inhibition: An overview. *Comput. Mol. Biol.* **2016**, *6*, 1.
5. Dolcet, X.; Llobet, D.; Pallares, J.; Matias-Guiu, X. NF-kB in development and progression of human cancer. *Virchows Arch.* **2005**, *446*, 475–482
6. Hellweg, C.E. The Nuclear Factor κB pathway: A link to the immune system in the radiation response. *Cancer Lett.* **2015**, *368*, 275–289.
7. Anilkumar, S.; Wright-Jin, E. NF-κB as an inducible regulator of inflammation in the central nervous system. *Cells* **2024**, *13*, 485.
8. Poladian, N.; Orujyan, D.; Narinyan, W.; Oganyan, A.K.; Navasardyan, I.; Velpuri, P.; Chorbajian, A.; Venketaraman, V. Role of NF-κB during Mycobacterium tuberculosis Infection. *Int. J. Mol. Sci.* **2023**, *24*, 1772.
9. Song, K.; Li, S. The role of ubiquitination in NF-κB signaling during virus infection. *Viruses* **2021**, *13*, 145.
10. Mohan, S.; Hakami, M.A.; Dailah, H.G.; Khalid, A.; Najmi, A.; Zoghebi, K.; Halawi, M.A.; Alotaibi, T.M. From inflammation to metastasis: The central role of miR-155 in modulating NF-κB in cancer. *Pathol.-Res. Pract.* **2024**, *253*, 154962.
11. Xue, J.; Yang, X.-R.; Wang, L. NF-κB signaling pathway in osteosarcoma: From signaling networks to targeted therapy. *Front. Oncol.* **2025**, *15*, 1565760.
12. Magné, N.; Toillon, R.-A.; Bottero, V.; Didelot, C.; Van Houtte, P.; Gérard, J.-P.; Peyron, J.-F. NF-κB modulation and ionizing radiation: Mechanisms and future directions for cancer treatment. *Cancer Lett.* **2006**, *231*, 158–168.
13. Serasanambati, M.; Chilakapati, S.R. Function of nuclear factor kappa B (NF-kB) in human diseases-a review. *South Indian J. Biol. Sci.* **2016**, *2*, 368–387.
14. Cui, C.; Yang, R.; Chen, H.; Li, D.; Sun, X.; Wang, Y.; Pan, Q. Air toxins disorder the NF-kB Pathway leads to immune disorders and immune diseases in the human health. *Ecotoxicol. Environ. Saf.* **2025**, *302*, 118474.
15. Smale, S.T. Luciferase assay. *Cold Spring Harb. Protoc.* **2010**, *2010*, pdb.prot5421.
16. Allard, S.T.; Kopish, K. Luciferase reporter assays: Powerful, adaptable tools for cell biology research. *Cell Notes* **2008**, *21*, 23–6.
17. Sherf, B.A.; Navarro, S.L.; Hannah, R.R.; Wood, K.V. Dual-luciferase reporter assay: An advanced co-reporter technology integrating firefly and Renilla luciferase assays. *Promega Notes* **1996**, *57*, 2–8.
18. Promega. *Dual-Luciferase® Reporter Assay System Technical Manual, TM-040*; Promega Corporation: Madison, WI, USA, revised 08/2023, accessed on 13 August 2025.
19. Kain, S.R.; Ganguly, S. Overview of genetic reporter systems. *Curr. Protoc. Mol. Biol.* **2004**, *68*, 9.6.1–9.6.12.
20. Naylor, L.H. Reporter gene technology: The future looks bright. *Biochem. Pharmacol.* **1999**, *58*, 749–757.
21. Hellweg, C.E.; Baumstark-Khan, C.; Horneck, G. Generation of stably transfected mammalian cell lines as fluorescent screening assay for NF-B activation-dependent gene expression. *J. Biomol. Screen.* **2003**, *8*, 511–521.
22. Hellweg, C.E.; Arenz, A.; Bogner, S.; Schmitz, C.; Baumstark-Khan, C. Activation of nuclear factor κB by different agents: Influence of culture conditions in a cell-based assay. *Ann. N. Y. Acad. Sci.* **2006**, *1091*, 191–204.
23. Hellweg, C.E.; Baumstark-Khan, C.; Schmitz, C.; Lau, P.; Meier, M.M.; Testard, I.; Berger, T.; Reitz, G. Activation of the nuclear factor κB pathway by heavy ion beams of different linear energy transfer. *Int. J. Radiat. Biol.* **2011**, *87*, 954–963.
24. Harrold, A.P.; Cleary, M.M.; Bharathy, N.; Lathara, M.; Berlow, N.E.; Foreman, N.K.; Donson, A.M.; Amani, V.; Zuercher, W.J.; Keller, C. In vitro benchmarking of NF-κB inhibitors. *Eur. J. Pharmacol.* **2020**, *873*, 172981.
25. Posit Team. *RStudio: Integrated Development Environment for R*, version 2025.5.1.513; Posit Software PBC: Boston, MA, USA, 2025. Available online: http://www.posit.co/ (accessed on 17 April 2025).
26. R Core Team. *R: A Language and Environment for Statistical Computing*, version 4.4.3; R Foundation for Statistical Computing: Vienna, Austria, 2025. Available online: https://www.R-project.org/ (accessed on 17 April 2025).
27. Lincoln, M. *clipr: Read and Write from the System Clipboard*, R Package Version 0.8.0.2022; R Foundation for Statistical Computing: Vienna, Austria, 2022. Available online: https://github.com/mdlincoln/clipr (accessed on 17 April 2025).
28. Zeileis, A.; Fisher, J.C.; Hornik, K.; Ihaka, R.; McWhite, C.D.; Murrell, P.; Stauffer, R.; Wilke, C.O. Colorspace: A Toolbox for Manipulating and Assessing Colors and Palettes. *J. Stat. Soft.* **2020**, *96*, 1–49.

29. Wickham, H.; François, R.; Henry, L.; Müller, K.; Vaughan, D. *dplyr: A Grammar of Data Manipulation*, R Package Version 1.1.4; R Foundation for Statistical Computing: Vienna, Austria, 2023. Available online: https://dplyr.tidyverse.org/ (accessed on 17 June 2025).
30. Ritz, C.; Baty, F.; Streibig, J.C.; Gerhard, D. Dose-Response Analysis Using R. *PLoS ONE* **2015**, *10*, e0146021
31. Wickham, H. *Forcats: Tools for Working with Categorical Variables (Factors)*, R Package version 1.0.0; R Foundation for Statistical Computing: Vienna, Austria, 2023. Available online: https://forcats.tidyverse.org (accessed on 17 June 2025).
32. Wickham, H. *ggplot2: Elegant Graphics for Data Analysis*, R Package version 3.5.2.; Springer-Verlag: New York, NY, USA, 2016. Available online: https://ggplot2.tidyverse.org/ (accessed on 17 April 2025).
33. Hester, J.; Bryan, J. *Glue: Interpreted String Literals*, R Package Version 1.8.0; R Foundation for Statistical Computing: Vienna, Austria, 2024. Available online: https://glue.tidyverse.org/ (accessed on 17 April 2025).
34. Grolemund, G.; Wickham, H. Dates and times made easy with lubridate. *J. Stat. Softw.* **2011**, *40*, 1–25.
35. Pedersen, T. *Patchwork: The Composer of Plots*, R Package version 1.3.2; R Foundation for Statistical Computing: Vienna, Austria, 2025. Available online: https://CRAN.R-project.org/package=patchwork (accessed on 6 September 2025).
36. Wickham, H. *purrr: Functional Programming Tools*, R Package version 1.1.0; R Foundation for Statistical Computing: Vienna, Austria, 2025. Available online: https://purrr.tidyverse.org/ (accessed on 1 August 2025).
37. Wickham, H.; Hester, J.; Bryan, J. *readr: Read Rectangular Text Data*, R Package version 2.1.5; R Foundation for Statistical Computing: Vienna, Austria, 2024. Available online: https://readr.tidyverse.org (accessed on 17 June 2025).
38. Wickham, H.; Bryan, J. *readxl: Read Excel Files*, R Package version 1.4.5; R Foundation for Statistical Computing: Vienna, Austria, 2025. Available online: https://readxl.tidyverse.org (accessed on 17 June 2025).
39. Ushey, K.; Wickham, H. *renv: Project Environments*, R package version 1.1.4; R Foundation for Statistical Computing: Vienna, Austria, 2025. Available online: https://CRAN.R-project.org/package=renv (accessed on 16 April 2025).
40. Wickham, H.; Pedersen, T.; Seidel, D. *scales: Scale Functions for Visualization*, R Package version 1.4.0; R Foundation for Statistical Computing: Vienna, Austria, 2025. Available online: https://scales.r-lib.org (accessed on 17 June 2025).
41. Wickham, H. *stringr: Simple, Consistent Wrappers for Common String Operations*, R Package version 1.5.1; R Foundation for Statistical Computing: Vienna, Austria, 2023. Available online: https://stringr.tidyverse.org (accessed on 17 April 2025).
42. Müller, K.; Wickham, H. *tibble: Simple Data Frames*, R Package version 3.3.0; R Foundation for Statistical Computing: Vienna, Austria, 2025. Available online: https://tibble.tidyverse.org/ (accessed on 17 June 2025).
43. Wickham, H.; Vaughan, D.; Girlich, M. *tidyr: Tidy Messy Data*, R Package version 1.3.1; R Foundation for Statistical Computing: Vienna, Austria, 2024. Available online: https://tidyr.tidyverse.org (accessed on 17 June 2025).
44. Wickham, H.; Averick, M.; Bryan, J.; Chang, W.; McGowan, L.D.; François, R.; Grolemund, G.; Hayes, A.; Henry, L.; Hester, J.; et al. Welcome to the Tidyverse. *J. Open Source Softw.* **2019**, *4*, 1686. https://doi.org/10.21105/joss.01686
45. Ooms, J. write*xl: Export Data Frames to Excel 'xlsx' Format*, R package version 1.5.4; R Foundation for Statistical Computing: Vienna, Austria, 2025. Available online: https://CRAN.R-project.org/package=writexl (accessed on 3 September 2025).
46. Graham, F.L.; Smiley, J.; Russell, W.C.; Nairn, R. Characteristics of a human cell line transformed by DNA from human adenovirus type 5. *J. Gen. Virol.* **1977**, *36*, 59–72.
47. Promega. *pGL4.32[luc2P/NF-κB-RE/Hygro] Vector Protocol, Part# 9PIE849*; Promega Corporation: Madison, WI, USA, 2025.
48. Sebaugh, J. Guidelines for accurate EC50/IC50 estimation. *Pharm. Stat.* **2011**, *10*, 128–134.
49. Brereton, R.G. CHEMOMETRICS AND STATISTICS|Signal Processing. In *Encyclopedia of Analytical Science*, 2nd ed.; Worsfold, P., Townshend, A., Poole, C., Eds.; Elsevier: Oxford, UK, 2005; pp. 46–51.
50. Nelson, D.; Ihekwaba, A.; Elliott, M.; Johnson, J.; Gibney, C.; Foreman, B.; Nelson, G.; Sée, V.; Horton, C.; Spiller, D. Oscillations in NF-κB signaling control the dynamics of gene expression. *Science* **2004**, *306*, 704–708.
51. Dorrington, M.G.; Fraser, I.D.C. NF-κB Signaling in Macrophages: Dynamics, Crosstalk, and Signal Integration. *Front. Immunol.* **2019**, *10*, 705.
52. Leclerc, G.M.; Boockfor, F.R.; Faught, W.J.; Frawley, L.S. Development of a destabilized firefly luciferase enzyme for measurement of gene expression. *Biotechniques* **2000**, *29*, 590–601.
53. Thompson, J.F.; Hayes, L.S.; Lloyd, D.B. Modulation of firefly luciferase stability and impact on studies of gene regulation. *Gene* **1991**, *103*, 171–177.
54. Ignowski, J.M.; Schaffer, D.V. Kinetic analysis and modeling of firefly luciferase as a quantitative reporter gene in live mammalian cells. *Biotechnol. Bioeng.* **2004**, *86*, 827–834.
55. Prescott, J.A.; Mitchell, J.P.; Cook, S.J. Inhibitory feedback control of NF-κB signalling in health and disease. *Biochem. J.* **2021**, *478*, 2619–2664.

56. Li, X.; Zhao, X.; Fang, Y.; Jiang, X.; Duong, T.; Fan, C.; Huang, C.-C.; Kain, S.R. Generation of destabilized green fluorescent protein as a transcription reporter. *J. Biol. Chem.* **1998**, *273*, 34970–34975.
57. Hellweg, C.E.; Arenz, A.; Baumstark-Khan, C. Assessment of space environmental factors by cytotoxicity bioassays. *Acta Astronaut.* **2007**, *60*, 525–533.
58. Thorne, N.; Inglese, J.; Auld, D.S. Illuminating insights into firefly luciferase and other bioluminescent reporters used in chemical biology. *Chem. Biol.* **2010**, *17*, 646–657.
59. Mazo-Vargas, A.; Park, H.; Aydin, M.; Buchler, N.E. Measuring fast gene dynamics in single cells with time-lapse luminescence microscopy. *Mol. Biol. Cell* **2014**, *25*, 3699–3708.
60. Mohanty, B. Promoter architecture and transcriptional regulation of genes upregulated in germination and coleoptile elongation of diverse rice genotypes tolerant to submergence. *Front. Genet.* **2021**, *12*, 639654.
61. Noursadeghi, M.; Tsang, J.; Haustein, T.; Miller, R.F.; Chain, B.M.; Katz, D.R. Quantitative imaging assay for NF-κB nuclear translocation in primary human macrophages. *J. Immunol. Methods* **2008**, *329*, 194–200.
62. Baeuerle, P.A.; Baltimore, D. IκB: A specific inhibitor of the NF-κB transcription factor. *Science* **1988**, *242*, 540–546.
63. Sanchez, A.; Garcia, H.G.; Jones, D.; Phillips, R.; Kondev, J. Effect of promoter architecture on the cell-to-cell variability in gene expression. *PLoS Comput. Biol.* **2011**, *7*, e1001100.
64. Rest, J.S.; Bullaughey, K.; Morris, G.P.; Li, W.-H. Contribution of transcription factor binding site motif variants to condition-specific gene expression patterns in budding yeast. *PLoS ONE* **2012**, *7*, e32274.
65. Natarajan, M.; Aravindan, N.; Meltz, M.; Herman, T. Post-translational modification of I-kappa B alpha activates NF-κB in human monocytes exposed to 56Fe ions. *Radiat. Environ. Biophys.* **2002**, *41*, 139–144.
66. Macaeva, E.; Tabury, K.; Michaux, A.; Janssen, A.; Averbeck, N.; Moreels, M.; De Vos, W.H.; Baatout, S.; Quintens, R. High-LET carbon and iron ions elicit a prolonged and amplified p53 signaling and inflammatory response compared to low-LET X-rays in human peripheral blood mononuclear cells. *Front. Oncol.* **2021**, *11*, 768493.
67. Feles, S.; Overath, C.; Reichardt, S.; Diegeler, S.; Schmitz, C.; Kronenberg, J.; Baumstark-Khan, C.; Hemmersbach, R.; Hellweg, C.E.; Liemersdorf, C. Streamlining culture conditions for the neuroblastoma cell line SH-SY5Y: A prerequisite for functional studies. *Methods Protoc.* **2022**, *5*, 58.
68. Dyer, B.W.; Ferrer, F.A.; Klinedinst, D.K.; Rodriguez, R. A noncommercial dual luciferase enzyme assay system for reporter gene analysis. *Anal. Biochem.* **2000**, *282*, 158–161.
69. Hampf, M.; Gossen, M. A protocol for combined Photinus and Renilla luciferase quantification compatible with protein assays. *Anal. Biochem.* **2006**, *356*, 94–99.
70. Spitta, L.F.; Diegeler, S.; Baumstark-Khan, C.; Hellweg, C.E. An in-vitro approach for water quality determination: Activation of NF-κB as marker for cancer-related stress responses induced by anthropogenic pollutants of drinking water. *Environ. Sci. Pollut. Res.* **2018**, *25*, 3985–3995.
71. Chishti, A.A.; Hellweg, C.E.; Berger, T.; Baumstark-Khan, C.; Feles, S.; Kätzel, T.; Reitz, G. Constitutive expression of tdTomato protein as a cytotoxicity and proliferation marker for space radiation biology. *Life Sci. Space Res.* **2015**, *4*, 35–45.
72. Zeuner, M.-T.; Vallance, T.; Vaiyapuri, S.; Cottrell, G.S.; Widera, D. Development and characterisation of a novel NF-κB reporter cell line for investigation of neuroinflammation. *Mediat. Inflamm.* **2017**, *2017*, 6209865.
73. Ducrest, A.L.; Amacker, M.; Lingner, J.; Nabholz, M. Detection of promoter activity by flow cytometric analysis of GFP reporter expression. *Nucleic Acids Res.* **2002**, *30*, e65.
74. McKinnon, K.M. Flow cytometry: An overview. *Curr. Protoc. Immunol.* **2018**, *120*, 5.1.1–5.1.11.
75. Feles, S.; Keßler, R.; Hauslage, J. Pioneering the Future of Experimental Space Hardware: MiniFix-a Fully 3D-Printed and Highly Adaptable System for Biological Fixation in Space. *Microgravity Sci. Technol.* **2025**, *37*, 22.
76. Thiel, C.S.; Tauber, S.; Seebacher, C.; Schropp, M.; Uhl, R.; Lauber, B.; Polzer, J.; Neelam, S.; Zhang, Y.; Ullrich, O. Real-time 3D high-resolution microscopy of human cells on the international space station. *Int. J. Mol. Sci.* **2019**, *20*, 2033.
77. Schell, M.T.; Spitzer, A.L.; Johnson, J.A.; Lee, D.; Harris, H.W. Heat shock inhibits NF-kB activation in a dose-and time-dependent manner. *J. Surg. Res.* **2005**, *129*, 90–93.
78. Heltberg, M.; von Borries, M.; Bendix, P.M.; Oddershede, L.B.; Jensen, M.H. Temperature Controls Onset and Period of NF-κ B Oscillations and can Lead to Chaotic Dynamics. *Front. Cell Dev. Biol.* **2022**, *10*, 910738.
79. Feles, S.; Holbeck, I.M.; Hauslage, J. From Lab to Launchpad: A Modular Transport Incubator for Controlled Thermal and Power Conditions of Spaceflight Payloads. *Instruments* **2025**, *9*, 21.
80. England, C.G.; Ehlerding, E.B.; Cai, W. NanoLuc: A small luciferase is brightening up the field of bioluminescence. *Bioconjug. Chem.* **2016**, *27*, 1175–1187.

81. Loh, J.M.; Proft, T. Comparison of firefly luciferase and NanoLuc luciferase for biophotonic labeling of group A Streptococcus. *Biotechnol. Lett.* **2014**, *36*, 829–834.
82. Boute, N.; Lowe, P.; Berger, S.; Malissard, M.; Robert, A.; Tesar, M. NanoLuc luciferase–a multifunctional tool for high throughput antibody screening. *Front. Pharmacol.* **2016**, *7*, 27.
83. Stierschneider, A.; Grünstäudl, P.; Colleselli, K.; Atzler, J.; Klein, C.T.; Hundsberger, H.; Wiesner, C. Light-inducible spatiotemporal control of TLR4 and NF-κB-Gluc reporter in human pancreatic cell line. *Int. J. Mol. Sci.* **2021**, *22*, 9232.
84. Yang, B.; Wagner, J.; Damaschke, N.; Yao, T.; Wuerzberger-Davis, S.M.; Lee, M.-H.; Svaren, J.; Miyamoto, S.; Jarrard, D.F. A novel pathway links oxidative stress to loss of insulin growth factor-2 (IGF2) imprinting through NF-κB activation. *PLoS ONE* **2014**, *9*, e88052.
85. Shaner, N.C.; Lambert, G.G.; Chammas, A.; Ni, Y.; Cranfill, P.J.; Baird, M.A.; Sell, B.R.; Allen, J.R.; Day, R.N.; Israelsson, M. A bright monomeric green fluorescent protein derived from Branchiostoma lanceolatum. *Nat. Methods* **2013**, *10*, 407–409.
86. Lam, A.J.; St-Pierre, F.; Gong, Y.; Marshall, J.D.; Cranfill, P.J.; Baird, M.A.; McKeown, M.R.; Wiedenmann, J.; Davidson, M.W.; Schnitzer, M.J. Improving FRET dynamic range with bright green and red fluorescent proteins. *Nat. Methods* **2012**, *9*, 1005–1012.
87. Chishti, A.A.; Baumstark-Khan, C.; Nisar, H.; Hu, Y.; Konda, B.; Henschenmacher, B.; Spitta, L.F.; Schmitz, C.; Feles, S.; Hellweg, C.E. The Use of ProteoTuner Technology to Study Nuclear Factor κB Activation by Heavy Ions. *Int. J. Mol. Sci.* **2021**, *22*, 13530.
88. Liu, S.; Su, Y.; Lin, M.Z.; Ronald, J.A. Brightening up biology: Advances in luciferase systems for in vivo imaging. *ACS Chem. Biol.* **2021**, *16*, 2707–2718.
89. Kim, S.-B.; Furuta, T. Bioluminescence from the bright and dark sides. *Front. Chem. Biol.* **2024**, *3*, 1459397.
90. Chishti, A.A.; Baumstark-Khan, C.; Koch, K.; Kolanus, W.; Feles, S.; Konda, B.; Azhar, A.; Spitta, L.F.; Henschenmacher, B.; Diegeler, S. Linear energy transfer modulates radiation-induced NF-kappa B activation and expression of its downstream target genes. *Radiat. Res.* **2018**, *189*, 354–370.
91. Hellweg, C.E.; Spitta, L.F.; Koch, K.; Chishti, A.A.; Henschenmacher, B.; Diegeler, S.; Konda, B.; Feles, S.; Schmitz, C.; Berger, T. The role of the nuclear factor κB pathway in the cellular response to low and high linear energy transfer radiation. *Int. J. Mol. Sci.* **2018**, *19*, 2220.

Disclaimer/Publisher's Note: The statements, opinions and data contained in all publications are solely those of the individual author(s) and contributor(s) and not of MDPI and/or the editor(s). MDPI and/or the editor(s) disclaim responsibility for any injury to people or property resulting from any ideas, methods, instructions or products referred to in the content.